Single Higgs boson production at electron-positron colliders in gauge-Higgs unification

Shuichiro Funatsu,[1] Hisaki Hatanaka,[2] Yuta Orikasa,[3] and Naoki Yamatsu[4,*]

[1]*Ushiku, Ibaraki 300-1234, Japan*
[2]*Osaka, Osaka 536-0014, Japan*
[3]*Institute of Experimental and Applied Physics, Czech Technical University in Prague, Husova 240/5, 110 00 Prague 1, Czech Republic*
[4]*Department of Physics, National Taiwan University, Taipei 10617, Taiwan, Republic of China*

(Received 19 January 2023; accepted 5 April 2023; published 26 April 2023)

We examine contributions to single Higgs boson production processes via Z' and W' bosons in the $SU(3)_C \times SO(5)_W \times U(1)_X$ gauge-Higgs unification (GHU) model. In particular, we analyze the cross sections of three single Higgs boson production processes $e^-e^+ \to Zh$, $e^-e^+ \to \nu\bar{\nu}h$, and $e^-e^+ \to e^-e^+h$ in the SM and the GHU model. For the Higgs strahlung process $e^-e^+ \to Zh$, we show that for a parameter region satisfying the current experimental constraints, a maximum deviation from the SM is about up to 6% for the center-of-mass energy of the initial electron and positron $\sqrt{s} = 250$ GeV and that from the SM is about up to 20% for $\sqrt{s} = 500$ GeV, depending on the initial polarization of electron and positron. The deviation from the SM is monotonically increasing with respect to $\sqrt{s}$ for $\sqrt{s} \lesssim 1$ TeV. By using the Higgs strahlung process, it is possible to explore up to the region of tens of TeV in terms of the Kaluza-Klein (KK) mass. We also show that the sign of the bulk mass of a lepton multiplet in the GHU model can be determined by examining the deviation of the left-right symmetry of the $e^-e^+ \to Zh$ process from the SM. The contributions to the cross sections of the $e^-e^+ \to \nu\bar{\nu}h$ and $e^-e^+ \to e^-e^+h$ processes via the Z' and W' bosons are relatively small compared to that for $e^-e^+ \to Zh$ at least for $\sqrt{s} \leq 1$ TeV. As is the same as in the SM, the $e^-e^+ \to \nu\bar{\nu}h$ process gives a main contribution to the single Higgs boson production processes for $\sqrt{s} \gtrsim 500$ GeV, but large deviations from the SM are only observed on energy scales close to the masses of the first KK gauge bosons or higher.

DOI: 10.1103/PhysRevD.107.075030

I. INTRODUCTION

The Standard Model (SM) in particle physics is well established at low energies. However, it is not yet clear whether the properties of the observed Higgs boson are exactly the same as those of the Higgs boson in the SM. Current and future experiments such as the Large Hadron Collider (LHC) [1,2], the High-Luminosity Large Hadron Collider (HL-LHC) [3], the International Linear Collider (ILC) [4–10], the Compact Linear Collider (CLIC) [11], the Future Circular Collider (FCC-hh, FCC-ee) [12,13], the Cool Copper Collider (C^3) [14], and Circular Electron Positron Collider (CEPC) [15] are needed to more precisely determine the couplings of the Higgs boson to quarks, leptons, and SM gauge bosons, as well as the self-coupling of the Higgs boson.

The SM Higgs boson sector remains unsatisfactory: the dynamics of the SM gauge bosons, the photon, the W and Z bosons, and the gluons, are governed by the gauge principle, but the dynamics of the SM Higgs boson is not governed by the gauge principle. The Higgs boson coupling of quarks and leptons and the self-coupling of the Higgs boson are also not governed by the principle. At the quantum level, there are large corrections to the mass of the Higgs boson. To reproduce the observed mass of the Higgs boson $m_h = 125.25 \pm 0.17$ GeV [16], an extremely strong cancellation between the bare mass and quantum effects must be required. One known way to stabilize the mass of the Higgs boson against quantum corrections is to identify the Higgs boson as the zero mode of the five-dimensional component of the gauge potential. This scenario is called gauge-Higgs unification (GHU) [17–22].

In GHU models, the Higgs boson appears as a fluctuating mode in the 5-dimensional (5D) Aharonov-Bohm (AB) phase θ_H; $SU(3)_C \times SO(5)_W \times U(1)_X$ GHU models in the Randall-Sundrum (RS) warped space are proposed in Refs. [23–26]. The phenomena of the GHU models below the electroweak (EW) scale are very close to those of the SM [26–36]. The gauge coupling constants of

*yamatsu@phys.ntu.edu.tw

quarks and leptons to the Z and W bosons in the GHU model differ by less than 0.1% from the coupling constants in the SM for the parameter region that satisfies the current experiments, i.e., the Kaluza-Klein (KK) mass $m_{\rm KK} \gtrsim 13$ TeV and the AB phase $\theta_H \lesssim 0.1$ [35]. The gauge coupling constants of the Higgs boson to the W and Z bosons are approximately equal to the corresponding coupling constants in the SM multiplied by $\cos\theta_H$. The coupling constants of the Higgs boson to the quarks and the leptons are approximately equal to those in the SM multiplied by $\cos\theta_H$ or $\cos^2(\theta_H/2)$ depending on the $SO(5)_W$ representations of the quarks and the leptons. The deviation of the coupling constants of the Higgs boson to the W and Z bosons, the quarks, and the leptons from the SM in the GHU model is less than 1% for $\theta_H \leq 0.1$ [32]. The decay of the Higgs boson to two photons in the GHU model is finite and very small, even when the contribution of KK excitation modes is taken into account [27]. The electroweak phase transition (EWPT) in the GHU model is a weakly first order phase transition [34], which is very similar to the EWPT in the SM [37].

The GHU models predict massive vector bosons Z' and W' bosons. The Z' bosons are mixed vector bosons of $U(1)_X$, $U(1)_L(\subset SU(2)_L)$, and $U(1)_R(\subset SU(2)_R)$, where $SU(2)_L \times SU(2)_R \subset SO(5)$. The W' bosons are mixed vector bosons of $SO(5)_W/(U(1)_L \times U(1)_R)$. The $SU(3)_C \times SO(5)_W \times U(1)_X$ GHU models can be roughly classified into two types of models depending on whether the $SO(5)_W$ representations of the quarks and the leptons are vector or spinor representations. The GHU model whose fermions belong to the spinor representation of $SO(5)_W$ [26,31–36] can be regarded as a low-energy effective description of the GHU model based on the $SO(11)$ grand unified gauge symmetry [38–44], where the SM gauge symmetry and field content are incorporated into grand unified theory (GUT) [45–50] in higher dimensional framework [51–65]. We focus on the spinor type model in this paper. In the GHU model, $\theta_H \lesssim 0.10$ and $m_{\rm KK} \gtrsim 13$ TeV are obtained as parameter constraints of the GHU model by using the Z' and W' boson search results for the $pp \to \ell\nu$ and $pp \to \ell^-\ell^+$ processes at the LHC at $\sqrt{s} = 13$ TeV with up to 140 fb^{-1} data [66–71].

The e^-e^+ collider experiment is capable of searching for signals in the GHU model up to the KK mass scale $m_{\rm KK}$ of tens of times the center-of-mass energy $\sqrt{s}$ of e^-e^+ [33,36,72–83]. Large parity violation appears in the couplings of quarks and leptons to KK gauge bosons, especially to the first KK modes. The sign of the bulk mass parameter of the fermions in the GHU model determines whether the coupling constants of the Z' and W' bosons to right- or left-handed fermions are larger. In Ref. [33], the SM and the GHU model are compared in detail for observables such as cross sections, forward-backward asymmetries [84,85], left-right asymmetries [84–87], and left-right forward-backward asymmetries [85,88–91] in the processes $e^-e^+ \to f\bar{f}$ ($f\bar{f} = \mu^-\mu^+, c\bar{c}, b\bar{b}, t\bar{t}$). For example, the total cross section of the $e^-e^+ \to \mu^-\mu^+$ process at $\sqrt{s} = 250$ GeV in the GHU model whose $m_{\rm KK} \simeq 13$ TeV and $\theta_H = 0.10$ is different at most about 3% compared to that in the SM, where it strongly depends on the initial polarizations of the electron and the positron. Due to the very large cross section of the fermion pair production processes, we can clearly observe deviations from the SM in the early stage of the ILC experiment ($\sqrt{s} = 250$ GeV, integral luminosity $L_{\rm int} = 250$ fb^{-1}) even when $m_{\rm KK}$ is slightly larger than the current experimental constraint $m_{\rm KK} \simeq 13$ TeV. The cross section of the Bhabha scattering $e^-e^+ \to e^-e^+$ process [92–96] is also very large, and the deviation from the SM in the GHU model can be also observed in the early-stage of the ILC experiment when $m_{\rm KK}$ is slightly larger than the current experimental constraint $m_{\rm KK} = 13$ TeV [36,77]. Furthermore, since the cross sections of the fermion pair production processes are very sensitive to the initial polarizations of the electron and the positron, the sign of the corresponding bulk mass of each fermion in each final state in the GHU model can also be determined by analyzing the polarization dependence.

To clarify the nature of the Higgs boson in the SM and the GHU model, it is essential to understand Higgs boson production processes. Since the mass of the SM Higgs boson is about 125 GeV, a Higgs strahlung process $e^-e^+ \to Zh$ is the main single Higgs boson production process for $\sqrt{s} \lesssim 500$ GeV, and the W^-W^+ gauge boson fusion process $e^-e^+ \to \nu\bar{\nu}W^{-*}W^{+*} \to \nu\bar{\nu}h$ is the main single Higgs boson production process for $\sqrt{s} \gtrsim 500$ GeV [10,97,98], where the contributions depend on the initial polarizations of the electron and the positron. There are the Z' and W' bosons in the GHU model, so these additional gauge bosons affect the Higgs boson production processes. The Higgs boson production processes in the GHU model have not been analyzed in detail. In particular, the dependence of the initial polarizations of the electron and the positron has not been discussed at all. In this paper, we analyze the cross sections and the left-right asymmetries of the $e^-e^+ \to Zh$ and $e^-e^+ \to f\bar{f}h$ ($f\bar{f} = \nu\bar{\nu}, e^-e^+$) in the SM and the GHU model within the Born approximation. The Higgs boson production processes in the SM have been analyzed not only in the Born approximation but also including quantum corrections [99–102]. The Higgs boson production processes in other models beyond the SM have been also discussed in e.g., Refs. [103–106].

In this paper, we consider three single Higgs boson production processes $e^-e^+ \to Zh$, $e^-e^+ \to \nu\bar{\nu}h$, and $e^-e^+ \to e^-e^+h$ to clarify the difference between the predictions of the cross sections in the SM and the GHU model. For the Higgs strahlung process $e^-e^+ \to Zh$, we show that for a parameter region satisfying the current experimental constraints, a maximum deviation from the SM is about up to 6% for $\sqrt{s} = 250$ GeV and that from the SM is about up to 20% for $\sqrt{s} = 500$ GeV, depending on

the initial polarization of the electron and the positron. The deviation from the SM is monotonically increasing when $\sqrt{s}$ is increasing for $\sqrt{s} \lesssim 1$ TeV. By using the Higgs strahlung process, it is possible to explore up to the region of tens of TeV in terms of the KK mass. We also show that the sign of the bulk mass of a lepton multiplet in the GHU model can be determined by examining the deviation of the left-right symmetry of the $e^-e^+ \to Zh$ process from the SM. The deviation of the left-right asymmetry of the $e^-e^+ \to Zh$ process from the SM in the GHU model can be large even when $\sqrt{s}$ is not so large. We show that the deviations of the $e^-e^+ \to \nu\bar{\nu}h$ and $e^-e^+ \to e^-e^+h$ processes from the SM in the GHU model are relatively small compared to the deviations of the $e^-e^+ \to Zh$ process at least for $\sqrt{s} \leq 1$ TeV.

The paper is organized as follows. In Sec. II, the $SU(3)_C \times SO(5)_W \times U(1)_X$ GHU model is introduced. In Sec. III, we give some parameter sets of the GHU model. In Sec. IV, we present numerical results for the cross sections of the three Higgs boson production processes $e^-e^+ \to Zh$, $e^-e^+ \to \nu\bar{\nu}h$, and $e^-e^+ \to e^-e^+h$. Section V is devoted to summary and discussions. In the Appendix, we give the formulas for the cross sections of the $e^-e^+ \to Zh$ and $e^-e^+ \to f\bar{f}h$ ($f\bar{f} = \nu_e\bar{\nu}_e, e^-e^+$) processes, involving the Z' and W' bosons as well as the Z and W bosons.

II. MODEL

In this paper, we focus on observables related with the EW gauge bosons and leptons at tree level. The $SU(3)_C$ gauge bosons and fermions except leptons are not directly involved, so we omit them. For the full field content in the GHU model, see Ref. [26], in which the $SU(3)_C \times SO(5)_W \times U(1)_X$ GHU model was originally proposed.

The GHU model is defined in the RS warped space with the following [107]:

$$ds^2 = g_{MN}dx^M dx^N = e^{-2\sigma(y)}\eta_{\mu\nu}dx^\mu dx^\nu + dy^2, \quad (2.1)$$

where $M, N = 0, 1, 2, 3, 5$, $\mu, \nu = 0, 1, 2, 3$, $y = x^5$, $\eta_{\mu\nu} = \mathrm{diag}(-1, +1, +1, +1)$, $\sigma(y) = \sigma(y + 2L) = \sigma(-y)$, and $\sigma(y) = ky$ for $0 \leq y \leq L$. By using the conformal coordinate $z = e^{ky}$ $(1 \leq z \leq z_L = e^{kL})$ in the region $0 \leq y \leq L$, the metric is rewritten by

$$ds^2 = \frac{1}{z^2}\left(\eta_{\mu\nu}dx^\mu dx^\nu + \frac{dz^2}{k^2}\right). \quad (2.2)$$

The bulk region $0 < y < L$ $(1 < z < z_L)$ is anti-de Sitter (AdS) spacetime with a cosmological constant $\Lambda = -6k^2$, which is sandwiched by the UV brane at $y = 0$ $(z = 1)$ and the IR brane at $y = L$ $(z = z_L)$. The KK mass scale is $m_{\mathrm{KK}} = \pi k/(z_L - 1)$.

A. Field content

The EW symmetry $SU(2)_L \times U(1)_Y$ is embedded into $SO(5)_W \times U(1)_X$ symmetry. The associated gauge fields of $SO(5)_W$ and $U(1)_X$ are denoted by $A_M^{SO(5)_W}$ and $A_M^{U(1)_X}$, respectively. The orbifold boundary conditions (BCs) P_j $(j = 0, 1)$ of the gauge fields on the UV brane $(y = 0)$ and the IR brane $(y = L)$ are given by

$$\begin{pmatrix} A_\mu \\ A_y \end{pmatrix}(x, y_j - y) = P_j \begin{pmatrix} A_\mu \\ -A_y \end{pmatrix}(x, y_j + y)P_j^{-1} \quad (2.3)$$

for each gauge field, where $(y_0, y_1) = (0, L)$. For the $U(1)_X$ gauge boson $A_M^{U(1)_X}$, $P_0 = P_1 = 1$. For the $SO(5)_W$ gauge boson $A_M^{SO(5)_W}$, $P_0 = P_1 = P_{\mathbf{5}}^{SO(5)_W}$, where $P_{\mathbf{5}}^{SO(5)_W} = \mathrm{diag}(I_4, -I_1)$. The orbifold BCs of the $SO(5)_W$ symmetry break $SO(5)_W$ to $SO(4)_W \simeq SU(2)_L \times SU(2)_R$. W, Z bosons and γ (photon) are zero modes in the $SO(5)_W \times U(1)_X$ of 4 dimensional (4D) gauge bosons, whereas the 4D Higgs boson is a zero mode in the $SO(5)_W/SO(4)_W$ part of the 5th dimensional gauge boson. In the GHU model, extra neutral gauge bosons Z' correspond to the KK photons $\gamma^{(n)}$, the KK Z bosons $Z^{(n)}$, and the KK Z_R bosons $Z_R^{(n)}$ $(n \geq 1)$, where the γ, and Z, Z_R bosons are the mass eigen states of the electro-magnetic (EM) $U(1)_{\mathrm{EM}}$ neutral gauge bosons of $SU(2)_L$, $SU(2)_R$, and $U(1)_X$. Extra charged gauge bosons W' correspond to the KK W boson $W^{\pm(n)}$ $(n \geq 1)$ and the KK W_R bosons $W_R^{\pm(n)}$ $(n \geq 1)$.

Leptons are introduced both in the 5D bulk and on the UV brane. They are listed in Table I. The SM lepton multiples are identified with the zero modes of the lepton multiplets $\Psi^\alpha_{(\mathbf{1},\mathbf{4})}$ $(\alpha = 1, 2, 3)$. The bulk fields $\Psi^\alpha_{(\mathbf{1},\mathbf{4})}$ obey the following BCs:

$$\Psi^\alpha_{(\mathbf{1},\mathbf{4})}(x, y_j - y) = -P_{\mathbf{4}}^{SO(5)_W}\gamma^5\Psi^\alpha_{(\mathbf{1},\mathbf{4})}(x, y_j + y), \quad (2.4)$$

where $P_{\mathbf{4}}^{SO(5)_W} = \mathrm{diag}(I_2, -I_2)$. With the BCs in Eq. (2.4), the parity assignment of the leptons is summarized in Table II. Neutral fermions are introduced as the brane fermions χ^α $(\alpha = 1, 2, 3)$ on the UV brane, which are responsible for reproducing tiny neutrino masses via the seesaw mechanism in the GHU model [42].

TABLE I. The field content for the lepton sector in the GHU model is shown.

	$(SU(3)_C \times SO(5)_W)_X$
Lepton	$(\mathbf{1},\mathbf{4})_{-\frac{1}{2}}$
Brane fermion	$(\mathbf{1},\mathbf{1})_0$
Brane scalar	$(\mathbf{1},\mathbf{4})_{\frac{1}{2}}$

TABLE II. Parity assignment $(P_0^{SO(5)_W}, P_1^{SO(5)_W})$ of the lepton multiplets in the bulk is shown. G_{22} stands for $SU(2)_L \times SU(2)_R (\subset SO(5)_W)$.

Field	$(SU(3)_C \times SO(5)_W)_X$	G_{22}	Left-handed	Right-handed	Name
$\Psi^{\alpha}_{(\mathbf{1},\mathbf{4})}$	$(\mathbf{1},\mathbf{4})_{-\frac{1}{2}}$	$[\mathbf{2},\mathbf{1}]$	$(+,+)$	$(-,-)$	$\nu_e\ \nu_\mu\ \nu_\tau$ $e\ \mu\ \tau$
		$[\mathbf{1},\mathbf{2}]$	$(-,-)$	$(+,+)$	$\nu'_e\ \nu'_\mu\ \nu'_\tau$ $e'\ \mu'\ \tau'$

The brane scalar field $\Phi_{(\mathbf{1},\mathbf{4})}(x)$ in Table I is responsible for breaking $SO(5)_W \times U(1)_X$ to $SU(2)_L \times U(1)_Y$. A spinor $\mathbf{4}$ of $SO(5)_W$ is decomposed into $[\mathbf{2},\mathbf{1}] \oplus [\mathbf{1},\mathbf{2}]$ of $SO(4)_W \simeq SU(2)_L \times SU(2)_R$. We assume that the brane scalar $\Phi_{(\mathbf{1},\mathbf{4})}$ develops a nonvanishing vacuum expectation value (VEV):

$$\Phi_{(\mathbf{1},\mathbf{4})} = \begin{pmatrix} \Phi_{[\mathbf{2},\mathbf{1}]} \\ \Phi_{[\mathbf{1},\mathbf{2}]} \end{pmatrix}, \qquad \langle \Phi_{[\mathbf{1},\mathbf{2}]} \rangle = \begin{pmatrix} 0 \\ w \end{pmatrix}, \tag{2.5}$$

which reduces the symmetry $SO(4)_W \times U(1)_X$ to the EW gauge symmetry $SU(2)_L \times U(1)_Y$. It is assumed that $w \gg m_{\mathrm{KK}}$, which ensures that the orbifold BCs for the 4D components of the $SU(2)_R \times U(1)_X/U(1)_Y$ gauge fields become effectively Dirichlet conditions at the UV brane [40]. Accordingly the mass of the neutral physical mode of $\Phi_{(\mathbf{1},\mathbf{4})}$ is much larger than m_{KK}.

The $U(1)_Y$ gauge boson is a mixed state of $U(1)_R$ $(\subset SU(2)_R)$ and $U(1)_X$ gauge bosons. The $U(1)_Y$ gauge field B_M^Y is given in terms of the $SU(2)_R$ gauge fields $A_M^{a_R}$ $(a_R = 1_R, 2_R, 3_R)$ and the $U(1)_X$ gauge field B_M by

$$B_M^Y = \sin\phi A_M^{3_R} + \cos\phi B_M. \tag{2.6}$$

Here the mixing angle ϕ between $U(1)_R$ and $U(1)_X$ is given by $\cos\phi = g_A/\sqrt{g_A^2 + g_B^2}$ and $\sin\phi = g_B/\sqrt{g_A^2 + g_B^2}$, where g_A and g_B are gauge couplings in $SO(5)_W$ and $U(1)_X$, respectively. The 4D $SU(2)_L$ gauge coupling is given by $g_w = g_A/\sqrt{L}$. The 5D gauge coupling constant $g_Y^{5\mathrm{D}}$ of $U(1)_Y$ and the 4D bare Weinberg angle at the tree level, θ_W^0, are given by

$$g_Y^{5\mathrm{D}} = \frac{g_A g_B}{\sqrt{g_A^2 + g_B^2}}, \qquad \sin\theta_W^0 = \frac{\sin\phi}{\sqrt{1 + \sin^2\phi}}. \tag{2.7}$$

The 4D Higgs boson $\phi_H(x)$ is the zero mode contained in the $A_z = (kz)^{-1}A_y$ component:

$$A_z^{(j5)}(x,z) = \frac{1}{\sqrt{k}}\phi_j(x)u_H(z) + \cdots, \qquad u_H(z) = \sqrt{\frac{2}{z_L^2 - 1}}z,$$
$$\phi_H(x) = \frac{1}{\sqrt{2}}\begin{pmatrix} \phi_2 + i\phi_1 \\ \phi_4 - i\phi_3 \end{pmatrix}. \tag{2.8}$$

Without loss of generality, we assume that $\langle\phi_1\rangle$, $\langle\phi_2\rangle, \langle\phi_3\rangle = 0$ and $\langle\phi_4\rangle \neq 0$, which is related to the AB phase θ_H in the fifth dimension by $\langle\phi_4\rangle = \theta_H f_H$, where $f_H = 2g_w^{-1}k^{1/2}L^{-1/2}(z_L^2 - 1)^{-1/2}$.

B. Action

The bulk part of the action for the EW gauge and lepton sectors is given by

$$S_{\mathrm{bulk}}^{\mathrm{EW+lepton}} = S_{\mathrm{bulk}}^{\mathrm{EW\ gauge}} + S_{\mathrm{bulk}}^{\mathrm{lepton}}, \tag{2.9}$$

where $S_{\mathrm{bulk}}^{\mathrm{EW\ gauge}}$ and $S_{\mathrm{bulk}}^{\mathrm{lepton}}$ are bulk actions of the EW gauge bosons and the leptons, respectively. The action of each gauge field, $A_M^{SO(5)_W}$ or $A_M^{U(1)_X}$, is given in the form

$$S_{\mathrm{bulk}}^{\mathrm{EW\ gauge}} = \int d^5x\sqrt{-\det G}\left[-\mathrm{tr}\left(\frac{1}{4}F^{MN}F_{MN} + \frac{1}{2\xi}(f_{\mathrm{gf}})^2 + \mathcal{L}_{\mathrm{gh}}\right)\right], \tag{2.10}$$

where $\sqrt{-\det G} = 1/kz^5$, $z = e^{ky}$, tr is a trace over all group generators for each group, and F_{MN} is a field strength defined by

$$F_{MN} \coloneqq \partial_M A_N - \partial_N A_M - ig[A_M, A_N] \tag{2.11}$$

with each 5D gauge coupling constant g. The second and third terms in Eq. (2.10) are the gauge fixing term and the ghost term given in Ref. [26], respectively.

Each lepton multiplet $\Psi^{\alpha}_{(\mathbf{1},\mathbf{4})}(x,y)$ in the bulk has its own bulk-mass parameter c_L^{α} $(\alpha = 1,\ 2,\ 3)$. The covariant derivative is given by

$$\mathcal{D}(c_L^{\alpha}) = \gamma^A e_A{}^M\left(D_M + \frac{1}{8}\omega_{MBC}[\gamma^B, \gamma^C]\right) - c_L^{\alpha}\sigma'(y),$$
$$D_M = \partial_M - ig_A A_M^{SO(5)_W} + i\frac{1}{2}g_B A_M^{U(1)_X}. \tag{2.12}$$

Here $\sigma'(y) \coloneqq d\sigma(y)/dy$ and $\sigma'(y) = k$ for $0 < y < L$. Then the action for the lepton sector in the bulk is given by

$$S_{\text{bulk}}^{\text{lepton}} = \int d^5x\sqrt{-\det G}\sum_{\alpha=1}^{3}\overline{\Psi^{\alpha}_{(\mathbf{1},\mathbf{4})}}\,\mathcal{D}(c_L^{\alpha})\Psi^{\alpha}_{(\mathbf{1},\mathbf{4})}, \tag{2.13}$$

where $\overline{\Psi^{\alpha}_{(\mathbf{1},\mathbf{4})}} = i{\Psi^{\alpha}_{(\mathbf{1},\mathbf{4})}}^{\dagger}\gamma^0$. By using $\check{\Psi}^{\alpha}_{(\mathbf{1},\mathbf{4})} \coloneqq \Psi^{\alpha}_{(\mathbf{1},\mathbf{4})}/z^2$, the bulk part of the fermion action is rewritten by

$$S_{\text{bulk}}^{\text{lepton}} = \int d^4x\int_1^{z_L}\frac{dz}{k}\sum_{\alpha=1}^{3}\overline{\check{\Psi}^{\alpha}_{(\mathbf{1},\mathbf{4})}} \times\left[\gamma^{\mu}D_{\mu} + k\left(\gamma^5 D_z - \frac{c_L^{\alpha}}{z}\right)\right]\check{\Psi}^{\alpha}_{(\mathbf{1},\mathbf{4})}. \tag{2.14}$$

The action for the brane scalar field $\Phi_{(\mathbf{1},\mathbf{4})}(x)$ is given by

$$S_{\text{brane}}^{\Phi} = \int d^5x\sqrt{-\det G}\,\delta(y)\{-(D_{\mu}\Phi_{(\mathbf{1},\mathbf{4})})^{\dagger}D^{\mu}\Phi_{(\mathbf{1},\mathbf{4})} - \lambda_{\Phi_{(\mathbf{1},\mathbf{4})}}(\Phi^{\dagger}_{(\mathbf{1},\mathbf{4})}\Phi_{(\mathbf{1},\mathbf{4})} - |w|^2)^2\}, \tag{2.15}$$

where

$$D_{\mu}\Phi_{(\mathbf{1},\mathbf{4})} = \left\{\partial_{\mu} - ig_A\sum_{\alpha=1}^{10}A_{\mu}^{\alpha}T^{\alpha} - i\frac{1}{2}g_B B_{\mu}\right\}\Phi_{(\mathbf{1},\mathbf{4})}. \tag{2.16}$$

Here $SO(5)_W$ generators $\{T^{\alpha}\}$ consist of $SU(2)_L$ and $SU(2)_R$ generators $\{T^{a_L}, T^{a_R}\}$ $(a = 1, 2, 3)$ and $SO(5)_W/SO(4)_W$ generators $\{T^{\hat{p}} = T^{p5}/\sqrt{2}\}$ $(p = 1, 2, 3, 4)$. The corresponding canonically normalized gauge fields are given by

$$A_M^{a_L} = \frac{1}{\sqrt{2}}\left(\frac{1}{2}\epsilon^{abc}A_M^{bc} + A_M^{a4}\right),$$
$$A_M^{a_R} = \frac{1}{\sqrt{2}}\left(\frac{1}{2}\epsilon^{abc}A_M^{bc} - A_M^{a4}\right), \qquad A_M^{\hat{p}} = A_M^{p5}. \tag{2.17}$$

B_M represents the $U(1)_X$ gauge field.

The action for the gauge-singlet brane fermion $\chi^{\alpha}(x)$ is given by

$$S_{\text{brane}}^{\chi} = \int d^5x\sqrt{-\det G}\,\delta(y)\left\{\frac{1}{2}\bar{\chi}^{\alpha}\gamma^{\mu}\partial_{\mu}\chi^{\alpha} - \frac{1}{2}M^{\alpha\beta}\bar{\chi}^{\alpha}\chi^{\beta}\right\}, \tag{2.18}$$

where $\chi^{\alpha}(x)$ satisfies the Majorana condition $\chi^c = \chi$;

$$\chi = \begin{pmatrix}\xi\\ \eta\end{pmatrix}, \qquad \chi^c = \begin{pmatrix}+\eta^c\\ -\xi^c\end{pmatrix} = e^{i\delta_C}\begin{pmatrix}+\sigma^2\eta^*\\ -\sigma^2\xi^*\end{pmatrix}. \tag{2.19}$$

On the UV brane, the brane interaction terms among the bulk leptons, the brane fermions, and the brane scalar are given by

$$S_{\text{brane}}^{\text{int}} = -\int d^5x\sqrt{-\det G}\,\delta(y)\{\tilde{\kappa}_{\mathbf{1}}^{\alpha\beta}\bar{\chi}^{\beta}\tilde{\Phi}^{\dagger}_{(\mathbf{1},\mathbf{4})}\Psi^{\alpha}_{(\mathbf{1},\mathbf{4})} + \text{H.c.}\}, \tag{2.20}$$

where $\tilde{\kappa}_{\mathbf{1}}^{\alpha\beta}$ is a coupling constant.

The nonvanishing VEV $\langle\Phi_{(\mathbf{1},\mathbf{4})}\rangle \neq 0$ generates brane mass terms on the UV brane from the interaction term in Eq. (2.20). Together with the Majorana mass term in Eq. (2.18) the brane fermion mass terms are given by

$$S_{\text{brane mass}}^{\text{fermion}} = \int d^5x\sqrt{-\det G}\,\delta(y)\left[-\frac{m_B^{\alpha\beta}}{\sqrt{k}}(\bar{\chi}^{\beta}\check{\nu}_R'^{\alpha} + \bar{\check{\nu}}_R'^{\alpha}\chi^{\beta}) - \frac{1}{2}M^{\alpha\beta}\bar{\chi}^{\alpha}\chi^{\beta}\right], \tag{2.21}$$

where $m_B^{\alpha\beta} = \tilde{\kappa}_{\mathbf{1}}^{\alpha\beta}w\sqrt{k}$.

The VEV of the brane scalar field $\langle\Phi_{(\mathbf{1},\mathbf{4})}\rangle \neq 0$ also generates additional brane mass terms for the 4D components of the $SO(5)_W \times U(1)_X$ gauge fields. It follows from Eq. (2.15) that

$$S_{\text{brane}}^{\text{gauge}} = \int d^5x\sqrt{-\det G}\,\delta(y)\left\{-\frac{g_A^2|w|^2}{4}(A_{\mu}^{1_R}A^{1_R\mu} + A_{\mu}^{2_R}A^{2_R\mu}) - \frac{(g_A^2+g_B^2)|w|^2}{4}A_{\mu}^{3'_R}A^{3'_R\mu}\right\}. \tag{2.22}$$

III. PARAMETER SETS

To evaluate cross sections and other observable quantities in single Higgs boson production processes $e^-e^+ \to Zh$, $e^-e^+ \to \nu\bar{\nu}h$, $e^-e^+ \to e^-e^+h$ at tree level in the GHU model, we need to know the masses, decay widths, and coupling constants of the gauge bosons, the Higgs boson, and the leptons. Parameters of the model are determined in the steps described in Ref. [33].

We present several parameter sets of the coupling constants of the leptons, which are necessary for the present analysis. In Sec. II, we gave only the 5D Lagrangian of the GHU model, but in the analysis, we use a 4D effective theory with KK mode expansion of the 5th dimension. By solving the equations of motions derived from the BCs of each 5D multiplet, we can obtain the mass spectra of 4D modes for each 5D field. Once mass spectra of a field are known, wave functions of the zero mode and the KK modes of the field can be determined by substituting mass spectra into the mode function of the field. Furthermore, coupling constants can be obtained by performing overlap integrals of the wave functions of the corresponding fields. For more details, see e.g., Ref. [26] for gauge boson and fermion mass formulas and wave functions and Ref. [32] for the Higgs boson mass and coupling formulas.

TABLE III. The name of the parameter set and the corresponding z_L, k, and $\sin^2\theta_W^0$ for each θ_H and $m_{\rm KK}$ are listed. In the SM, $\sin^2\theta_W(\overline{\rm MS}) = 0.23122 \pm 0.00004$ [16]. The column "Name" denotes each parameter set.

Name	θ_H [rad]	$m_{\rm KK}$ [TeV]	z_L	k [GeV]	$\sin^2\theta_W^0$
A_-	0.10	13.00	3.865×10^{11}	1.599×10^{15}	0.2306
A_+	0.10	13.00	4.029×10^{11}	1.667×10^{15}	0.2318
B_-	0.07	19.00	1.420×10^{12}	8.589×10^{15}	0.2309
B_+	0.07	19.00	1.452×10^{12}	8.779×10^{15}	0.2315
C_-	0.05	25.00	5.546×10^{10}	4.413×10^{14}	0.2310
C_+	0.05	25.00	5.600×10^{10}	4.456×10^{14}	0.2313

We will describe the steps to fix parameter sets in the GHU model, where we will show parameter sets for leptons, the gauge bosons, and the Higgs boson.

(1) We pick the values of θ_H and $m_{\rm KK} = \pi k(z_L - 1)^{-1}$. From the constraints on θ_H and $m_{\rm KK}$ from the LHC-Run 2 results in the GHU model [35], we only consider parameters satisfying $\theta_H \leq 0.10$ and $m_{\rm KK} \geq 13$ TeV.

(Note that possible values of $m_{\rm KK}$ are restricted with given θ_H [32]. For example, for $\theta_H = 0.10$ $z_L \geq 10^{8.1}$ to reproduce the top quark mass, and $z_L \leq 10^{15.5}$ to realize the EW symmetry breaking. They lead to $m_{\rm KK} \simeq [11, 15]$ TeV.)

(2) k is determined in order for the Z boson mass m_Z to be reproduced, which fixes the warped factor z_L as well. (For the mass formula of Z boson, see Ref. [26].)

(3) The bare Weinberg angle θ_W^0 in the GHU model is given in Eq. (2.7). For each value of θ_H, the value of θ_W^0 is determined self-consistently to fit the observed forward-backward asymmetry $A_{\rm FB}(e^-e^+ \to \mu^-\mu^+) = 0.0169 \pm 0.0013$ at $\sqrt{s} = m_Z$ [16,108], after evaluating the coupling constants of the muon to the Z boson with the procedure described below. We have checked that each self-consistent value of θ_W^0 is found after a couple of iterations of this process.

The parameter sets of $(\theta_H, m_{\rm KK})$, named $A_\pm$,$B_\pm$, and $C_\pm$, used in this analysis are summarized in Table III, where the subscripts denote the sign of the bulk masses of the leptons. For example, A_+ denotes the case where the bulk mass of the lepton is positive and A_- denotes the case where the bulk mass of the lepton is negative.

(4) With given $\sin\theta_W^0$, wave functions of the gauge bosons are fixed. Masses and widths of Z', W, W' bosons are listed for each parameter set in Table IV. Although information on parameters of the quark sector is also needed when we determine the decay widths of the gauge bosons, the specific values of the parameters of the quark sector are omitted since they are not directly used in this analysis. The parameters of the quark sector are obtained by the same procedure as for the lepton sector. (For more detail, see Ref. [26].)

(5) The bulk masses of the leptons c_L^α in Eq. (2.14) are determined so as to reproduce the masses of charged leptons, where we denote c_L^1, c_L^2, c_L^3 as c_e, c_μ, c_τ. We use the masses of the electron, the muon, and the tau lepton given by $m_e = 0.48657$ MeV, $m_\mu = 102.72$ MeV, and $m_\tau = 1.7462$ GeV at $\mu = m_Z$ [109]. The parameters of the Majorana mass terms and brane interactions in the neutrino sector in Eq. (2.21), $M^{\alpha\beta}$ and $m_B^{\alpha\beta}$, are determined so as to

TABLE IV. Masses and widths of Z', W, W' bosons are listed for each parameter set listed in Table III. In the SM, $\alpha_{\rm EM} = 1/128$ at the mass scale of Z boson, $m_Z = 91.1876$ GeV, $\Gamma_Z = 2.4952$ GeV, $m_W = 80.377 \pm 0.012$ GeV, $\Gamma_W = 2.085 \pm 0.042$ GeV, [16]. The column "Name" denotes each parameter set in Table III. m_V and Γ_V ($V = Z^{(1)}, Z_R^{(1)}, W, W^{(1)}, W_R^{(1)}$) are the mass and decay width of each V boson, respectively. Decay widths are calculated by using the formulas in Ref. [33], where all possible two-body final states are taken into account.

Name	$m_{Z^{(1)}}$ [TeV]	$\Gamma_{Z^{(1)}}$ [TeV]	$m_{Z_R^{(1)}}$ [TeV]	$\Gamma_{Z_R^{(1)}}$ [TeV]	m_W [GeV]	Γ_W [GeV]	$m_{W^{(1)}}$ [TeV]	$\Gamma_{W^{(1)}}$ [TeV]	$m_{W_R^{(1)}}$ [TeV]	$\Gamma_{W_R^{(1)}}$ [TeV]
A_-	10.196	7.840	9.951	0.816	79.98	2.02	10.196	9.802	9.951	0.359
A_+	10.196	5.982	9.951	0.775	79.92	2.01	10.196	7.163	9.951	0.358
B_-	14.886	11.962	14.544	1.231	79.97	2.02	14.886	14.970	14.544	0.549
B_+	14.886	9.162	14.544	1.168	79.94	2.02	14.886	10.979	14.544	0.548
C_-	19.648	14.006	19.137	1.505	79.96	2.03	19.648	17.502	19.137	0.639
C_+	19.648	10.700	19.137	1.432	79.95	2.02	19.648	12.784	19.137	0.638

TABLE V. The bulk masses of electron, muon, and tau lepton, c_e, c_μ, c_τ and the brane interaction parameters of leptons $M_\ell, m_{B_e}, m_{B_{m}u}, m_{B_\tau}$ are listed. In the SM, $m_e = 0.48657$ MeV, $m_\mu = 102.72$ MeV, and $m_\tau = 1.7462$ GeV at $\mu = m_Z$ [109]. We take the neutrino masses: $m_{\nu_e} = m_{\nu_\mu} = m_{\nu_\tau} = 10^{-12}$ GeV. The column "Name" denotes each parameter set in Table III.

Name	c_e	c_μ	c_τ	M_ℓ [GeV]	m_{Be} [GeV]	$m_{B\mu}$ [GeV]	$m_{B\tau}$ [GeV]
A_-	−1.0067	−0.7929	−0.6753	10^6	4.834×10^5	1.342×10^8	2.949×10^9
A_+	+1.0058	+0.7924	+0.6750	10^6	8.382×10^{22}	6.373×10^{22}	4.931×10^{22}
B_-	−0.9828	−0.7791	−0.6670	10^6	4.952×10^5	1.375×10^8	3.021×10^9
B_+	+0.9824	+0.7788	+0.6669	10^6	3.017×10^{23}	2.294×10^{23}	1.775×10^{23}
C_-	−1.0469	−0.8162	−0.6893	10^6	4.652×10^5	1.292×10^8	2.838×10^9
C_+	+1.0467	+0.8161	+0.6982	10^6	1.165×10^{22}	8.857×10^{21}	6.853×10^{21}

reproduce the neutrino masses. The neutrino masses cannot be completely fixed because only two mass-squared differences are known from observations [16]. In our analysis, we take $m_{\nu_e} = m_{\nu_\mu} = m_{\nu_\tau} = 10^{-12}$ GeV for reference. For simplicity we assume that $M^{\alpha\beta}$ and $m_B^{\alpha\beta}$ are diagonal to the flavor. We take $M^{\alpha\beta} = M_\ell \delta_{\alpha\beta}$ $(\alpha, \beta = 1, 2, 3)$, $m_B^{11} = m_{B_e}$, $m_B^{22} = m_{B_\mu}$, $m_B^{33} = m_{B_\tau}$, and $m_B^{\alpha\beta} = 0$ for $\alpha \neq \beta$. The neutrino masses are so small that a difference of one to two orders of magnitude in their masses will not affect the results of this analysis. Neutrino mixings are ignored, but they do not affect the present analysis. The bulk masses and the brane interaction parameters of the leptons are listed in Table V.

In Table V, it may be problematic that the mass parameters $m_{B\ell}(\ell = e, \mu, \tau)$ of the brane fermions are larger than the Planck mass for the cases of positive bulk masses of the leptons. Furthermore, it has been pointed out in Ref. [26] that the appearance of extra vector-like neutrinos with MeV-scale masses is for the case of the positive bulk masses of the

TABLE VI. Coupling constants of charged vector bosons, $W, W'(= W^{(1)}, W_R^{(1)})$ bosons, to leptons in units of $g_w/\sqrt{2}$ are listed. The fine structure constant is the same as in the SM: $\alpha(M_Z)^{-1} = 127.951 \pm 0.009$ [16]. In the SM, $g_w = e/\sin\theta_W$, while in the GHU $g_w = e/\sin\theta_W^0$. The coupling constants of W boson to leptons in the SM are $g^L_{We\nu_e} = 1$. When the value is less than 10^{-4}, we write 0.

Name	$g^L_{We\nu_e}$	$g^R_{We\nu_e}$	$g^L_{W^{(1)}e\nu_e}$	$g^R_{W^{(1)}e\nu_e}$	$g^L_{W_R^{(1)}e\nu_e}$	$g^R_{W_R^{(1)}e\nu_e}$
A_-	+0.9976	0	+5.7451	0	+0.0145	0
A_+	+0.9988	0	−0.2220	0	0	0
B_-	+0.9988	0	+5.8583	0	+0.0073	0
B_+	+0.9994	0	−0.2171	0	0	0
C_-	+0.9994	0	+5.5706	0	+0.0035	0
C_+	+0.9997	0	−0.2316	0	0	0

Name	$g^L_{W\mu\nu_\mu}$	$g^R_{W\mu\nu_\mu}$	$g^L_{W^{(1)}\mu\nu_\mu}$	$g^R_{W^{(1)}\mu\nu_\mu}$	$g^L_{W_R^{(1)}\mu\nu_\mu}$	$g^R_{W_R^{(1)}\mu\nu_\mu}$
A_-	+0.9976	0	+5.4705	0	+0.0139	0
A_+	+0.9988	0	−0.2222	0	0	0
B_-	+0.9988	0	+5.5850	0	+0.0069	0
B_+	+0.9994	0	−0.2171	0	0	0
C_-	+0.9994	0	+5.2941	0	+0.0034	0
C_+	+0.9997	0	−0.2316	0	0	0

Name	$g^L_{W\tau\nu_\tau}$	$g^R_{W\tau\nu_\tau}$	$g^L_{W^{(1)}\tau\nu_\tau}$	$g^R_{W^{(1)}\tau\nu_\tau}$	$g^L_{W_R^{(1)}\tau\nu_\tau}$	$g^R_{W_R^{(1)}\tau\nu_\tau}$
A_-	+0.9976	0	+5.2878	0	+0.0134	0
A_+	+0.9988	0	−0.2217	0	0	0
B_-	+0.9988	0	+5.4046	0	+0.0067	0
B_+	+0.9994	0	−0.2169	0	0	0
C_-	+0.9994	0	+5.1077	0	+0.0032	0
C_+	+0.9997	0	−0.2314	0	0	0

leptons. The sign of the bulk masses causes a qualitative difference in the behavior of the coupling constants of fermions to the KK gauge bosons, so in this paper we consider the parameter sets of the positive bulk masses of the leptons as well as the negative bulk masses of the leptons for reference.

(6) With given the bulk masses and the brane interaction parameters, wave functions of fermions are fixed.

(7) The mass and self-coupling constant of the Higgs boson can be obtained from the effective potential of the Higgs boson [32]. The mass of the Higgs boson is determined by adjusting the bulk mass of the dark fermions so that the mass of the Higgs boson is $m_h = 125.25 \pm 0.17$ GeV [16].

To evaluate cross sections for single Higgs boson production processes such as $e^-e^+ \to Zh$, $e^-e^+ \to \nu\bar{\nu}h$, $e^-e^+ \to e^-e^+h$, we need to know not only the masses and the decay widths but also coupling constants of the gauge bosons, the Higgs boson, and the leptons. They are obtained from the five-dimensional gauge interaction terms by substituting the wave functions of gauge bosons and fermions or the Higgs boson and integrating over the fifth-dimensional coordinate [28–30].

(i) The coupling constants of the gauge bosons to the leptons are obtained by performing overlap integrals of the wave functions in the fifth dimension of gauge bosons and leptons. Coupling constants of gauge bosons to leptons are listed in Tables VI–VIII.

As can be seen from Tables VI–VIII the coupling constants of the zero modes and the 1st KK modes of the Z and W bosons to the zero modes of the leptons in the GHU are very close to those in the SM. More specifically, the deviations from the SM are less than 1%. There is almost no difference in the coupling constants of the Z and W bosons to the leptons for the positive and negative bulk masses of the leptons, while there is a large difference in the coupling constants of the KK gauge bosons, $Z'(= Z^{(1)}, Z_R^{(1)})$ and $W'(= W^{\pm(1)}, W_R^{\pm(1)})$ bosons, to the zero modes of the leptons. When the bulk masses of leptons are negative, the coupling constants of the 1st KK gauge bosons to the zero modes of the left-handed leptons are large, and those of the 1st KK gauge bosons to the zero modes of the right-handed leptons are small. On the other hand, when the bulk masses of the leptons are positive, the coupling constants of the 1st KK gauge bosons to the zero modes of the right-handed leptons are large and those of the 1st KK gauge bosons to the zero modes of the left-handed leptons are small.

TABLE VII. Coupling constants of neutral vector bosons, $Z, Z'(= Z^{(1)}, Z_R^{(1)})$ bosons, to neutrinos in units of $g_w = e/\sin\theta_W^0$ are listed. The coupling constants of Z boson to neutrinos in the SM are $(g^L_{Z_\nu}, g^R_{Z_\nu}) = (0.5703, 0)$ in units of g_w. Other information is the same as in Table VI.

Name	$g^L_{Z\nu_e}$	$g^R_{Z\nu_e}$	$g^L_{Z^{(1)}\nu_e}$	$g^R_{Z^{(1)}\nu_e}$	$g^L_{Z_R^{(1)}\nu_e}$	$g^R_{Z_R^{(1)}\nu_e}$
A_-	+0.5687	0	+3.2774	0	−1.0322	0
A_+	+0.5691	0	−0.1264	0	0	0
B_-	+0.5695	0	+3.3413	0	−1.0586	0
B_+	+0.5697	0	−0.1237	0	0	0
C_-	+0.5698	0	+3.1768	0	−1.0099	0
C_+	+0.5699	0	−0.1320	0	0	0

Name	$g^L_{Z\nu_\mu}$	$g^R_{Z\nu_\mu}$	$g^L_{Z^{(1)}\nu_\mu}$	$g^R_{Z^{(1)}\nu_\mu}$	$g^L_{Z_R^{(1)}\nu_\mu}$	$g^R_{Z_R^{(1)}\nu_\mu}$
A_-	+0.5687	0	+3.1207	0	−0.9852	0
A_+	+0.5691	0	−0.1264	0	0	0
B_-	+0.5695	0	+3.1854	0	−1.0114	0
B_+	+0.5697	0	−0.1237	0	0	0
C_-	+0.5698	0	+3.0191	0	−0.9623	0
C_+	+0.5699	0	−0.1320	0	0	0

Name	$g^L_{Z\nu_\tau}$	$g^R_{Z\nu_\tau}$	$g^L_{Z^{(1)}\nu_\tau}$	$g^R_{Z^{(1)}\nu_\tau}$	$g^L_{Z_R^{(1)}\nu_\tau}$	$g^R_{Z_R^{(1)}\nu_\tau}$
A_-	+0.5691	0	+3.0165	0	−0.9539	0
A_+	+0.5687	0	−0.1262	0	0	0
B_-	+0.5695	0	+3.0825	0	−0.9803	0
B_+	+0.5697	0	−0.1236	0	0	0
C_-	+0.5698	0	+2.9129	0	−0.9302	0
C_+	+0.5699	0	−0.1319	0	0	0

TABLE VIII. Coupling constants of neutral vector bosons, Z, Z' bosons, to charged leptons in units of $g_w = e/\sin\theta_W^0$ are listed. The coupling constants of Z boson to charged leptons in the SM are $(g^L_{Z_e}, g^R_{Z_e}) = (-0.3065, 0.2638)$ in units of g_w. Other information is the same as in Table VI.

Name	g^L_{Ze}	g^R_{Ze}	$g^L_{Z^{(1)}e}$	$g^R_{Z^{(1)}e}$	$g^L_{Z^{(1)}_R e}$	$g^R_{Z^{(1)}_R e}$
A_-	−0.3058	+0.2629	−1.7621	−0.0584	−1.0444	0
A_+	−0.3060	+0.2631	+0.0680	+1.5171	0	+1.3826
B_-	−0.3062	+0.2633	−1.7964	−0.0572	−1.0646	0
B_+	−0.3063	+0.2634	+0.0665	+1.5459	0	+1.4102
C_-	−0.3064	+0.2634	−1.7082	−0.0610	−1.0128	0
C_+	−0.3065	+0.2635	+0.0710	+1.4690	0	+1.3428

Name	$g^L_{Z\mu}$	$g^R_{Z\mu}$	$g^L_{Z^{(1)}\mu}$	$g^R_{Z^{(1)}\mu}$	$g^L_{Z^{(1)}_R \mu}$	$g^R_{Z^{(1)}_R \mu}$
A_-	−0.3058	+0.2629	−1.6778	−0.0584	−0.9969	0
A_+	−0.3060	+0.2631	+0.0680	+1.4447	0	+1.3197
B_-	−0.3062	+0.2633	−1.7126	−0.0572	−1.0173	0
B_+	−0.3063	+0.2634	+0.0665	+1.4738	0	+1.3474
C_-	−0.3064	+0.2634	−1.6234	−0.0610	−0.9651	0
C_+	−0.3065	+0.2635	+0.0710	+1.3961	0	+1.2796

Name	$g^L_{Z\tau}$	$g^R_{Z\tau}$	$g^L_{Z^{(1)}\tau}$	$g^R_{Z^{(1)}\tau}$	$g^L_{Z^{(1)}_R \tau}$	$g^R_{Z^{(1)}_R \tau}$
A_-	−0.3058	+0.2629	−1.6218	−0.0584	−0.9652	0
A_+	−0.3060	+0.2631	+0.0679	+1.3965	0	+1.2778
B_-	−0.3062	+0.2633	−1.6473	−0.0571	−0.9859	0
B_+	−0.3063	+0.2634	+0.0664	+1.4262	0	+1.3060
C_-	−0.3064	+0.2634	−1.5663	−0.0610	−0.9330	0
C_+	−0.3065	+0.2635	+0.0710	+1.3470	0	+1.2370

(ii) The coupling constants of gauge bosons to the Higgs boson are obtained by performing overlap integrals of the wave functions in the fifth dimension of gauge bosons and the Higgs boson. Coupling constants of gauge bosons to Higgs boson are listed Table IX.

From Table IX, the coupling constants of the Z and W bosons to the Higgs boson in the GHU model are very close to those in the SM. More specifically, the deviations from the SM are less than 1%.

TABLE IX. Coupling constants of gauge bosons to Higgs boson in units of g_w are listed. In the SM, $g_{WWh}/g_w = m_W = 80.38$ GeV and $g_{ZZh}/g_w = m_Z/\cos\theta_W = 104.00$ GeV. When the value is less than 0.1, we write 0.

Name	g_{WWh} [GeV]	$g_{WW^{(1)}h}$ [GeV]	$g_{W^{(1)}W^{(1)}h}$ [GeV]	$g_{WW^{(1)}_R h}$ [GeV]	$g_{W^{(1)}_R W^{(1)}_R h}$ [GeV]	$g_{W^{(1)}W^{(1)}_R h}$ [GeV]
A_-	+79.60	+395.80	−315.90	+405.14	0	−156.05
A_+	+79.54	+395.81	−315.62	+405.14	0	−155.92
B_-	+79.78	+406.12	−315.67	+414.29	0	−155.67
B_+	+79.75	+406.12	−315.53	+414.29	0	−155.60
C_-	+79.87	+381.16	−318.16	+389.29	0	−156.69
C_+	+79.85	+381.17	−318.80	+389.29	0	−156.65

Name	g_{ZZh} [GeV]	$g_{ZZ^{(1)}h}$ [GeV]	$g_{Z^{(1)}Z^{(1)}h}$ [GeV]	$g_{ZZ^{(1)}_R h}$ [GeV]	$g_{Z^{(1)}_R Z^{(1)}_R h}$ [GeV]	$g_{Z^{(1)}Z^{(1)}_R h}$ [GeV]
A_-	+103.47	+514.84	−410.55	+386.81	0	−148.87
A_+	+103.55	+515.66	−410.82	+386.56	0	−148.64
B_-	+103.74	+528.25	−410.43	+395.33	0	−148.48
B_+	+103.78	+528.67	−410.57	+395.20	0	−148.37
C_-	+103.86	+495.76	−414.64	+371.38	0	−149.45
C_+	+103.88	+495.96	−414.71	+371.32	0	−149.39

We comment on the expected improvement in the accuracy of the Weinberg angle in the ILC experiment. At the moment we use $A_{\rm FB}(e^-e^+ \to \mu^-\mu^+)$ to determine the value of the Weinberg angle θ_W^0. If the uncertainty of $A_{\rm FB}(e^-e^+ \to \mu^-\mu^+)$ is reduced by future experiments, we can use exactly the same method to determine the parameters. If the uncertainty of $A_{\rm FB}(e^-e^+ \to \mu^-\mu^+)$ is reduced by a factor of $1/10$, the uncertainty of $\sin^2\theta_W^0$ is also reduced by a factor of about $1/10$. However, the (unpolarized) forward-backward asymmetry $A_{\rm FB}$ is not a direct observable in the ILC experiment with polarized electrons and positrons. Although it is possible to obtain $A_{\rm FB}$ by combining observables, it is known that the accuracy of Weinberg angle determination can be improved by using more direct observables, polarization asymmetry parameters $A_f (f = e, \mu, \ldots)$ [10,16]. The relations between the Weinberg angle and the asymmetry parameters are approximately given as

$$A_f \simeq 8\left(\frac{1}{4} - |Q_f| \sin^2\theta_{\rm eff}^f\right). \tag{3.1}$$

From this relationship, the accuracy of $\sin^2\theta_{\rm eff}^f$ is estimated to be $1/8$ times the decision accuracy of A_f. This is also true for $\sin^2\theta_W^0$ in the GHU model. At present, the accuracy of $\sin^2\theta_W^0$ is $O(0.1)\%$ by using the currently forward-backward asymmetry $A_{\rm FB}(e^-e^+ \to \mu^-\mu^+)$. We expect that the decision accuracy of $\sin^2\theta_W^0$ will be $O(0.01)\%$ by using the expected accuracy of the asymmetry parameter A_e at the ILC experiment with $\sqrt{s} = 250$ GeV and $L_{\rm int} = 2$ ab^{-1} [10]; $O(0.001)\%$ by using the expected accuracy of the asymmetry parameter A_e at the ILC experiment with $\sqrt{s} = m_Z \simeq 91.2$ GeV and $L_{\rm int} = 100$ fb^{-1} [10].

IV. NUMERICAL ANALYSIS

We calculate cross sections of single Higgs boson production processes. More specifically, we analyze three processes $e^-e^+ \to Zh$, $e^-e^+ \to \nu\bar{\nu}h$, $e^-e^+ \to e^-e^+h$ for the initial states of unpolarized and polarized electrons and positrons, where we use the formula of the cross sections given in the Appendix. For the values of the initial polarizations, we mainly use $(P_{e^-}, P_{e^+}) = (\mp 0.8, \pm 0.3)$ with the ILC experiment in mind.

A. $e^-e^+ \to Zh$

Here we evaluate observables of the $e^-e^+ \to Zh$ process in the SM and the GHU model at tree level. We use the parameter sets $A_\pm$, $B_\pm$, $C_\pm$ listed in Tables III–IX.

In Fig. 1, we show the $\sqrt{s}$ dependence of the total cross sections of the $e^-e^+ \to Zh$ process in wider range of $\sqrt{s}$ in the SM and the GHU model with unpolarized $e^\pm$ beams. The calculation incorporates contributions up to the 1st KK mode. Above the first KK mass scale, the contributions from higher KK modes cannot be neglected, and the region where the calculation is reliable and valid for this analysis is well below the first KK mass scale. The left figure in Fig. 1 shows $\sigma^{Zh}(P_{e^-}, P_{e^+})$ given in Eq. (A14) in the SM and the GHU model with $(P_{e^-}, P_{e^+}) = (0, 0)$, where $A_\pm$, $B_\pm$, $C_\pm$ are the names of the parameter sets listed in Table III. The right figure shows $\sigma^{Zh}(P_{e^-}, P_{e^+})$ in the SM and GHU models with the initial states of polarized and unpolarized electron and positron. U, L, R stand $(P_{e^-}, P_{e^+}) = (0, 0), (-0.8, +0.3), (+0.8, -0.3)$, respectively.

From Fig. 1, in the $\sqrt{s} \lesssim O(1)$ TeV region, the cross sections in the GHU model are smaller than the cross sections in the SM, independent of the parameter sets and initial polarizations. From the right figure, we find that the deviations from the SM for each initial polarization of $e^\pm$

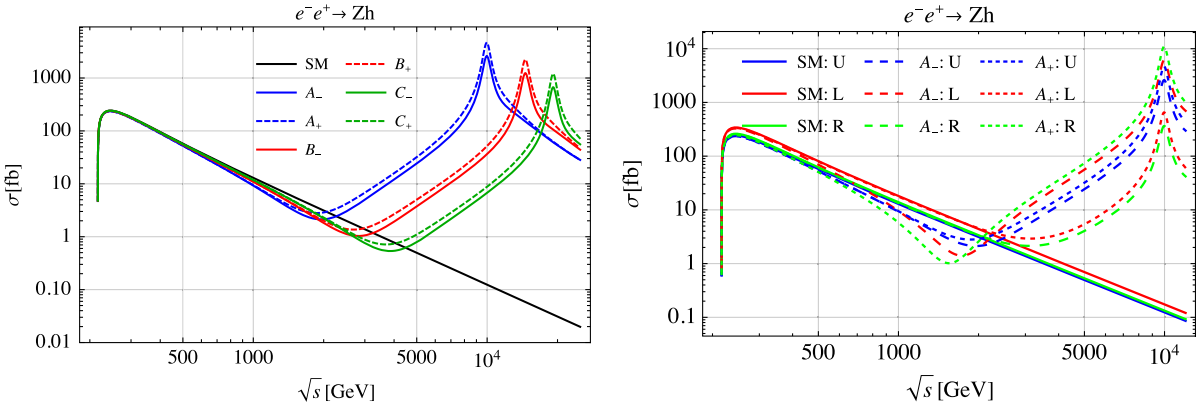

FIG. 1. The total cross sections of the $e^-e^+ \to Zh$ process in the SM and the GHU model are shown in wider range of $\sqrt{s}$. The left figure shows the $\sqrt{s}$ dependence of $\sigma^{Zh}(P_{e^-} = 0, P_{e^+} = 0)$ in the SM and the GHU model with unpolarized electron and positron beams, where $A_\pm$, $B_\pm$, $C_\pm$ are the names of the parameter sets listed in Table III. The right figure shows the $\sqrt{s}$ dependence of $\sigma^{Zh}(P_{e^-}, P_{e^+})$ in the SM and the GHU model whose parameter sets are $A_\pm$ with the three different polarizations U, L, R, where U, L, R stand for $(P_{e^-}, P_{e^+}) = (0, 0), (-0.8, +0.3), (+0.8, -0.3)$, respectively.

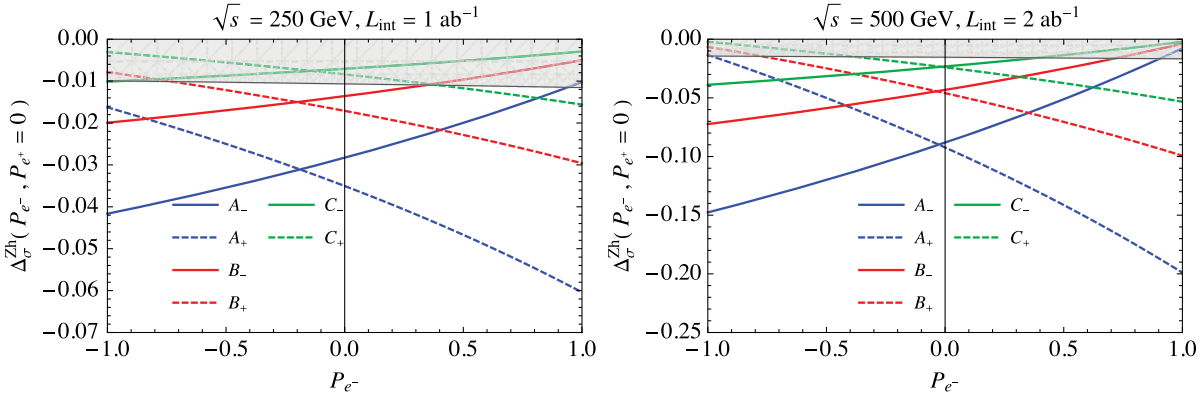

FIG. 2. The electron polarization dependence of the deviation from the SM in the GHU models for the total cross sections, $\Delta_\sigma^{Zh}(P_{e^-}, P_{e^+})$, is shown, where we fix $P_{e^+} = 0$. The gray region represents the 1σ statistical error estimated by using the decay mode of Z to $\mu^-\mu^+$, where in the first and second figures, we used the sets of the center-of-mass energies and the integrated luminosity $(\sqrt{s}, L_{\rm int}) = (250\ {\rm GeV}, 1\ {\rm ab}^{-1}), (500\ {\rm GeV}, 2\ {\rm ab}^{-1})$, respectively. Note that ${\rm Br}(Z \to \mu^-\mu^+) = (3.3662 \pm 0.0066)\%$ [16].

beams depend on the sign of the bulk masses. The deviation from the SM is monotonically increasing with respect to $\sqrt{s}$ for $\sqrt{s} \lesssim 1$ TeV. The cross sections in the GHU model are smaller than those in the SM because of the interference effects between the Z boson and the KK gauge bosons, and the cross sections in the GHU begin to increase in the energy scale region where the contributions to the cross sections from the KK gauge bosons are larger than the contribution to the cross section from the interference effects, indicating a turning point located at $\sqrt{s} \simeq \sqrt{m_Z m_{\rm KK}}$, where $m_{\rm KK} = 13$, 19, 25 TeV for the parameter sets $A_\pm$, $B_\pm$, $C_\pm$, respectively.

In Fig. 2, the electron polarization dependence of the deviation from the SM in the GHU models for the total cross sections, $\Delta_\sigma^{Zh}(P_{e^-}, P_{e^+})$, is shown, where $\Delta_\sigma^{Zh}(P_{e^-}, P_{e^+})$ is given in Eq. (A17). The 1σ statistical errors are estimated by using the decay mode of the Z boson to μ^- and μ^+, where ${\rm Br}(Z \to \mu^-\mu^+) = (3.3662 \pm 0.0066)\%$ [16]. We use the sets of the center-of-mass energies and the integrated luminosity $(\sqrt{s}, L_{\rm int}) = (250\ {\rm GeV}, 1\ {\rm ab}^{-1})$, $(500\ {\rm GeV}, 2\ {\rm ab}^{-1})$, respectively. For reference, here we consider only the decay channel of the Z boson to a pair of the muons [98]. In the ILC experiment, smaller statistical errors may be available by using the decay channel of the Z boson to hadron jets [10,98].

In Fig. 3, the $\sqrt{s}$ dependence of the left-right asymmetry A_{LR}^{Zh} of the $e^-e^+ \to Zh$ processes and the deviation from the SM $\Delta_{A_{LR}}^{Zh}$ are shown, where A_{LR}^{Zh} and $\Delta_{A_{LR}}^{Zh}$ are given in Eqs. (A18) and (A23), respectively. The 1σ statistical error in the SM at each $\sqrt{s}$ with 1 ab^{-1} for each polarized initial electron and positron $(P_{e^-}, P_{e^+}) = (\mp 0.8, \pm 0.3)$ is estimated by using the decay mode of Z to $\mu^-\mu^+$.

From Fig. 3, we find that for $\sqrt{s} \lesssim 2$ TeV, the left-right asymmetry A_{LR}^{Zh} in the GHU model is larger than that in the SM when the bulk mass of the leptons is positive, while

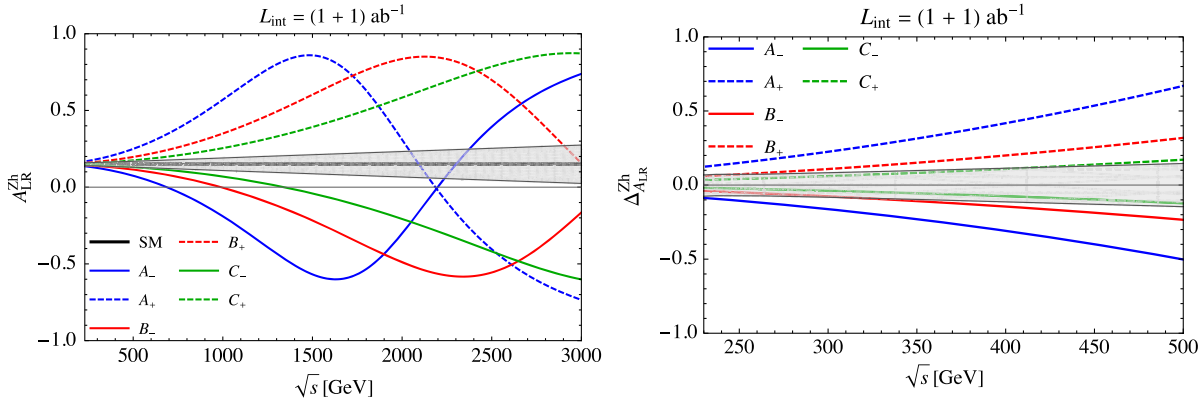

FIG. 3. The $\sqrt{s}$ dependence of the left-right asymmetry of the $e^-e^+ \to Zh$ process and the deviation from the SM are shown. The left figure shows the $\sqrt{s}$ dependence of A_{LR}^{Zh} in the SM and the GHU model. The right figure shows the $\sqrt{s}$ dependence of $\Delta_{A_{LR}}^{Zh}$. The energy ranges $\sqrt{s}$ in the first and second figures are $\sqrt{s} = [200, 3000]$ GeV, $\sqrt{s} = [200, 1000]$ GeV, respectively. The gray region represents the 1σ statistical error in the SM at each $\sqrt{s}$ with 1 ab^{-1} for each polarized initial states $(P_{e^-}, P_{e^+}) = (\mp 0.8, \pm 0.3)$ by using the decay mode of Z to $\mu^-\mu^+$. Other information is the same as in Fig. 2.

A_{LR}^{Zh} in the GHU model is smaller that in the SM when the bulk mass of the leptons is negative. As can be seen from Table IX, there is almost no bulk mass dependence for the coupling constants of the Higgs boson to the W and Z bosons in the SM and the GHU model, and the cubic coupling constants of the Z boson, the $Z'(=Z^{(1)}, Z_R^{(1)})$ boson, and the Higgs boson, $g_{ZZ^{(1)}h}$ and $g_{ZZ_R^{(1)}h}$, are larger than the cubic coupling constant of the Z boson, the Z boson, and the Higgs boson, g_{ZZh}. From Tables VI–VIII, there is almost no dependence on the sign of the bulk masses for the coupling constants of zero modes of the charged leptons to the zero mode of the Z boson, while there is large difference between the zero modes of the right-handed and left-handed leptons to the 1st KK modes of the Z and Z_R bosons. Some gauge coupling constants of the zero modes of the right-handed or left-handed leptons to the 1st KK modes of the Z' bosons $Z^{(1)}$ and $Z_R^{(1)}$ are larger than those of zero modes of the leptons to the zero mode of the Z boson.

In summary, for the $e^-e^+ \to Zh$ process, some of the coupling constants of the Z' bosons to the leptons and the Higgs boson are much larger than the coupling constants of the Z boson to the leptons and the Higgs boson, so that even a center-of-mass energy $\sqrt{s}$ that is an order of magnitude smaller than the masses of the Z' bosons can yield experimentally verifiable predictions.

B. $e^-e^+ \to \nu\bar{\nu}h$

Here we calculate the total cross sections of the $e^-e^+ \to \nu\bar{\nu}h$ process given in Eq. (A43), where if ν has no subscript, the contribution of all flavors shall be considered. Since neutrinos are not observable experimentally, we add up the contributions not only from the $e^-e^+ \to \nu_e\bar{\nu}_e h$ process but also from the $e^-e^+ \to \nu_\mu\bar{\nu}_\mu h$ and $e^-e^+ \to \nu_\tau\bar{\nu}_\tau h$ processes. In the SM, the contributions to $\sigma(e^-e^+ \to \nu_\mu\bar{\nu}_\mu h)$ and $\sigma(e^-e^+ \to \nu_\tau\bar{\nu}_\tau h)$ come only from the processes $\sigma(e^-e^+ \to Z \to Zh \to \nu_\mu\bar{\nu}_\mu h)$ and $\sigma(e^-e^+ \to Z \to Zh \to \nu_\tau\bar{\nu}_\tau h)$, respectively. When we ignore the neutrino masses in the SM, $\sum_{\ell=e,\mu,\tau}\sigma(e^-e^+ \to Z \to Zh \to \nu_\ell\bar{\nu}_\ell h) = 3\sigma(e^-e^+ \to Z \to Zh \to \nu_e\bar{\nu}_e h)$. In the GHU model, the coupling constants of the Z boson to the neutrinos given in Table VII are almost the same regardless of neutrino flavor. Therefore, to a very good approximation, the following relationship holds: $\sum_{\ell=e,\mu,\tau}\sigma(e^-e^+ \to Z \to Zh \to \nu_\ell\bar{\nu}_\ell h) \simeq 3\sigma(e^-e^+ \to Z \to Zh \to \nu_e\bar{\nu}_e h)$.

In Fig. 4, the total cross sections of the $e^-e^+ \to \nu\bar{\nu}h$ process with unpolarized and polarized electron and positron beams in the SM and the GHU model whose parameter sets are $A_\pm$, $B_\pm$, $C_\pm$ are showed up to the energy scale $\sqrt{s}$ where resonances due to the KK gauge boson can be confirmed. The left figure shows the $\sqrt{s}$ dependence of the total cross sections with unpolarized electron and positron beams in the SM and the GHU model whose parameter sets are $A_\pm$, $B_\pm$, $C_\pm$. The right figure shows the $\sqrt{s}$ dependence of the total cross sections with polarized electron and positron beams for the SM and the GHU model whose parameter sets are $A_\pm$. In both the figures, the main contribution to the peak around $\sqrt{s} \simeq 250$ GeV comes from the $e^-e^+ \to Z \to Zh \to \nu\bar{\nu}h$ process, and the main contributions to the peaks around $O(10)$ TeV come from the $e^-e^+ \to Z'(=Z^{(1)}, Z_R^{(1)}) \to Zh \to \nu\bar{\nu}h$ process for each parameter set. In our calculation, we take into account the contribution to the cross section from the W and Z bosons and the 1st KK gauge bosons $W^{\pm(1)}$, $W_R^{\pm(1)}$, $Z^{(1)}$, and $Z_R^{(1)}$ but the contribution from higher KK modes cannot be ignored above $O(m_{\rm KK})$. We verify that for the $e^-e^+ \to \nu\bar{\nu}h$ process the contribution from the KK gauge bosons is small, independent of the KK masses and the initial polarization of

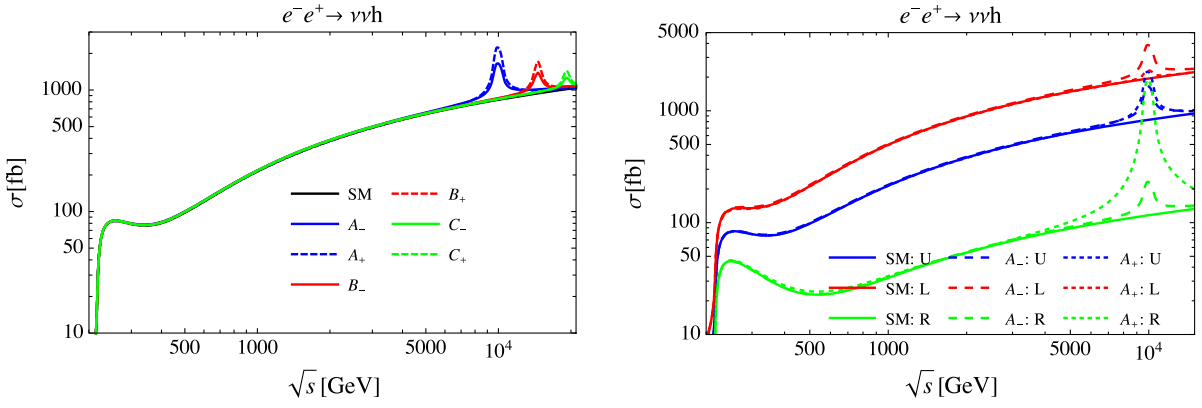

FIG. 4. The $\sqrt{s}$ dependence of the total cross sections of the $e^-e^+ \to \nu\bar{\nu}h$ process with unpolarized and polarized electron and positron beams in the SM and the GHU model is shown. The left figure shows the $\sqrt{s}$ dependence of the total cross sections with unpolarized electron and positron beams in the SM and the GHU model whose parameter sets are $A_\pm$, $B_\pm$, $C_\pm$. The right figure shows the $\sqrt{s}$ dependence of the total cross sections with unpolarized and polarized electron and positron beams in the SM and the GHU model whose parameter sets are $A_\pm$. The energy ranges $\sqrt{s}$ in the left and right figures are $\sqrt{s} = [200, 21000]$ GeV and $\sqrt{s} = [200, 15000]$ GeV, respectively. U, L, R stand $(P_{e^-}, P_{e^+}) = (0, 0), (-0.8, +0.3), (+0.8, -0.3)$, respectively.

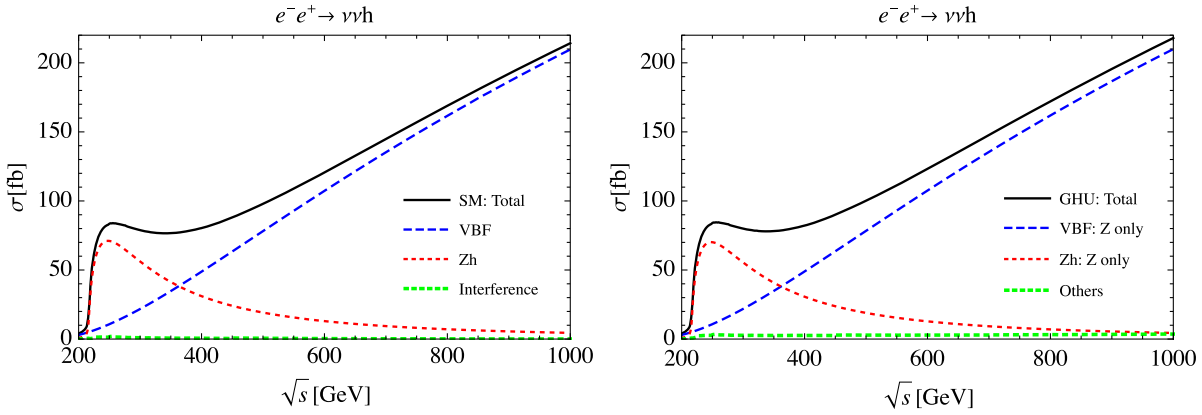

FIG. 5. The $\sqrt{s}$ dependence of the total cross sections of the $e^-e^+ \to \nu\bar{\nu}h$ process with unpolarized electron and positron beams is shown. The left figure shows the $\sqrt{s}$ dependence of the cross sections for total, vector boson fusion (VBF) only, Zh only, and interference between VBF and Zh processes only in the SM. The right figure shows the $\sqrt{s}$ dependence of the cross sections for total, VBF from Z boson, Zh from Z boson, and the others without VBF and Zh only from Z boson in the GHU model with the parameter set A_-. The others includes such as VBF and Zh including at least one KK mode. The energy ranges $\sqrt{s}$ in the figures are $\sqrt{s} = [200, 1000]$ GeV.

the electron and the positron, except around the Z' boson mass scale. Since the coupling constants of the W and Z bosons to the left-handed leptons are different from that of the W and Z bosons to the right-handed leptons, the cross section depend on the initial polarizations of the electron and the positron. Furthermore, since the parity violation of the W boson to the leptons are larger than that of the Z boson to the leptons, the vector boson fusion (VBF) process, in which the W boson gives the main contribution, depends more strongly on the initial polarizations than the Zh process, in which the Z boson gives the main contribution. The coupling constants of the Z' bosons to the leptons depend on the sign o the bulk masses. When the bulk mass is negative, the coupling constants to the left-handed fermions is larger, and when the bulk mass is positive, the coupling constant to the right-handed fermions is larger. As a result, the magnitude of the cross section by polarization at resonance energies strongly depends on the sign of the bulk mass.

In Fig. 5, the $\sqrt{s}$ dependence of the total cross sections of the $e^-e^+ \to \nu\bar{\nu}h$ process with unpolarized electron and positron beams in the SM and the GHU model whose parameter set is A_- is shown up to $\sqrt{s} = 1$ TeV. The contributions to the total cross sections from the VBF, Zh, and interference (other) in the SM and the GHU model are decomposed and displayed in the left and right figures, respectively. There is almost no difference between the cross sections in the SM and the GHU model for $\sqrt{s} \leq 1$ TeV. In both the SM and the GHU model, the main contribution comes from the Zh process below $\sqrt{s} \simeq 350$ GeV, while the

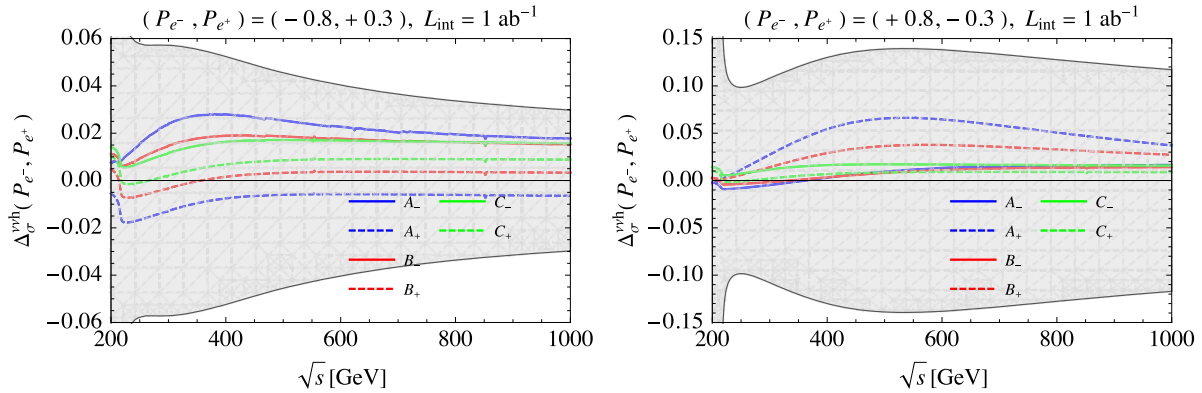

FIG. 6. The $\sqrt{s}$ dependence of the deviation from the SM in the GHU model with six parameter sets $A_\pm$, $B_\pm$, $C_\pm$ for total cross sections $\Delta_\sigma^{\nu\nu h}(P_{e^-}, P_{e^+})$ is shown. The left and right figures show the center-of-mass energies $\sqrt{s} = [200, 1000]$ GeV and $(P_{e^-}, P_{e^+}) = (-0.8, +0.3)$ and $(+0.8, -0.3)$, respectively. The gray regions represent the 1σ statistical errors in the SM at each $\sqrt{s}$ with 1 ab^{-1} by using the decay mode of the Higgs boson h to two photons $\gamma\gamma$, where the branching ratio for the SM Higgs boson with $m_H = 125$ GeV is given by $\mathrm{Br}(h \to \gamma\gamma) = 2.27(1 \pm 0.021) \times 10^{-3}$ [16].

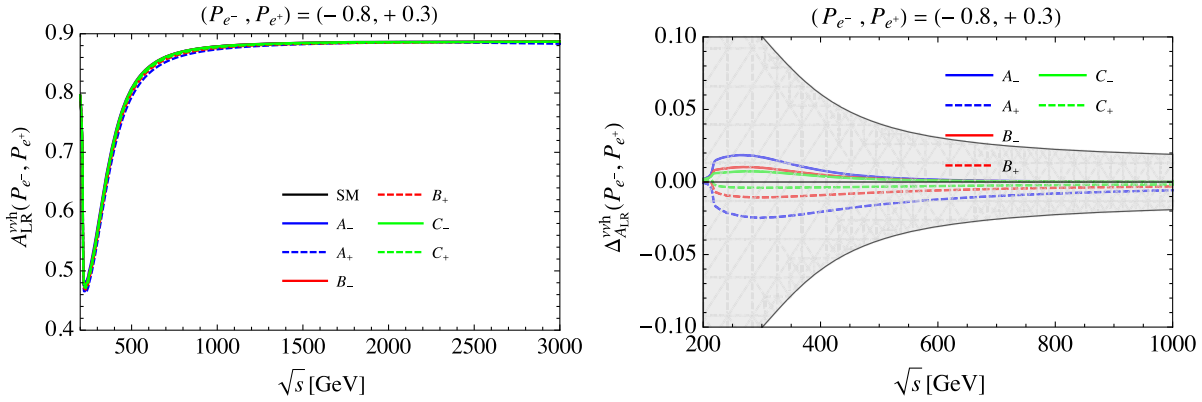

FIG. 7. The left-right asymmetry of the $e^-e^+ \to \nu\bar{\nu}h$ process $A^{\nu\nu h}_{LR}(P_{e^-}, P_{e^+})$ in the SM and the GHU model and the deviation of the left-right asymmetry from the SM in the GHU model $\Delta^{\nu\nu h}_{A_{LR}}(P_{e^-}, P_{e^+})$ are shown. The left and right figures show the $\sqrt{s}$ dependence of $A^{\nu\nu h}_{LR}(P_{e^-}, P_{e^+})$ and $\Delta^{\nu\nu h}_{A_{LR}}(P_{e^-}, P_{e^+})$ with the polarization $(P_{e^-}, P_{e^+}) = (-0.8, +0.3)$ and the six parameter sets $A_\pm$, $B_\pm$, $C_\pm$. The energy ranges $\sqrt{s}$ in the left and right figures are $\sqrt{s} = [200, 3000]$ GeV, $\sqrt{s} = [200, 1000]$ GeV, respectively. The gray region represents the statistical error explained in Table VI.

main contribution comes from the VBF process above $\sqrt{s} \simeq 350$ GeV, where the contributions from the Zh and VBF processes depend on the initial polarizations of the electron and the positron.

In Fig. 6, the $\sqrt{s}$ dependence of the deviation from the SM in the GHU model with six parameter sets $A_\pm$, $B_\pm$, $C_\pm$ for the total cross sections $\Delta^{\nu\nu h}_\sigma$ are shown, where $\Delta^{ffh}_\sigma(P_{e^-}, P_{e^+})$ is given in Eq. (A45). The left and right figures show the center-of-mass energies $\sqrt{s} = [200, 1000]$ GeV and $(P_{e^-}, P_{e^+}) = (-0.8, +0.3)$ and $(+0.8, -0.3)$, respectively. The 1σ statistical errors are estimated in the SM at each $\sqrt{s}$ with 1 ab^{-1} by using the decay mode of the Higgs boson h to two photons $\gamma\gamma$, where the branching ratio for the SM Higgs boson with $m_H = 125$ GeV is given by $\mathrm{Br}(h \to \gamma\gamma) = 2.27(1 \pm 0.021) \times 10^{-3}$ [16]. The branching ratio of the Higgs boson to the final state of the muon pair, whose energy and momentum can be well observed experimentally with high precision, is very small, where $\mathrm{Br}(h \to \mu^-\mu^+) = 2.18(1 \pm 0.017) \times 10^{-4}$ [16]. We refer to the decay of the Higgs boson to two photons, but the analysis of the signal by hadron jets in the ILC experiment is currently in progress. The mass reconstruction of the Higgs boson by using bottom quark pairs and τ lepton pairs may be available, which have much larger branching ratios of the Higgs boson, where $\mathrm{Br}(h \to b\bar{b}) = 5.82(1 \pm 0.013) \times 10^{-1}$ and $\mathrm{Br}(h \to \tau^-\tau^+) = 6.27(1 \pm 0.016) \times 10^{-2}$ [16]. If so, the deviation from the SM in the GHU model can be explored by using the $e^-e^+ \to \nu\bar{\nu}h$ process.

In Fig. 7, the $\sqrt{s}$ dependence of the left-right asymmetry of the $e^-e^- \to \nu\bar{\nu}h$ process $A^{\nu\nu h}_{LR}(P_{e^-}, P_{e^+})$ and the deviation of the left-right asymmetry from the SM $\Delta^{\nu\nu h}_{A_{LR}}(P_{e^-}, P_{e^+})$ with $(P_{e^-}, P_{e^+}) = (-0.8, +0.3)$ are shown, where $A^{\nu\nu h}_{LR}(P_{e^-}, P_{e^+})$ and $\Delta^{\nu\nu h}_{A_{LR}}(P_{e^-}, P_{e^+})$ are given in Eqs. (A46) and (A48), respectively. From Eq. (A47), when $(P_{e^-}, P_{e^+}) = (\mp 0.8, \pm 0.3)$ and $\sigma^{\nu\nu h}_{LL} \gg \sigma^{\nu\nu h}_{RR}, \sigma^{\nu\nu h}_{LR}, \sigma^{\nu\nu h}_{RL}$, we find $A^{\nu\nu h}_{LR}(P_{e^-} = -0.8, P_{e^+} = +0.3) \simeq 0.887$. Thus, we confirmed that when $\sqrt{s}$ is sufficiently large, the main contribution to the $e^-e^+ \to \nu\bar{\nu}h$ process comes almost exclusively from the VBF processes. Furthermore, the deviation from the SM becomes smaller when $\sqrt{s}$ is larger. Therefore, it it very difficult to confirm the deviation from the SM by using the left-right asymmetry of the $e^-e^+ \to \nu\bar{\nu}h$ process.

C. $e^-e^+ \to e^-e^+h$

Here we calculate the total cross section of the $e^-e^+ \to e^-e^+h$ process given in Eq. (A43). The cross section of the $e^-e^+ \to e^-e^+h$ process is smaller than that of the $e^-e^+ \to \nu\bar{\nu}h$ process in all energy regions unless the initial polarization of the electron (the positron) is extremely right-handed (left-handed). Therefore, this process is usually a subdominant Higgs boson production process.

The following figures in this subsection are made by using exactly the same formula and calculations as those in the previous subsection IV B, except for the difference between the final and intermediate state particles, and their coupling constants. The explanation of the figures is basically the same as in the previous section. We will omit duplicated explanations.

In Fig. 8, the $\sqrt{s}$ dependence of the total cross sections of the $e^-e^+ \to e^-e^+h$ process with unpolarized and polarized electron and positron beams in the SM and the GHU model are showed. The left figure shows the $\sqrt{s}$ dependence of the total cross sections with unpolarized electron and positron beams in the SM and the GHU model whose parameter sets are $A_\pm$, $B_\pm$, $C_\pm$. The right figure shows the $\sqrt{s}$ dependence of the total cross sections with polarized electron and

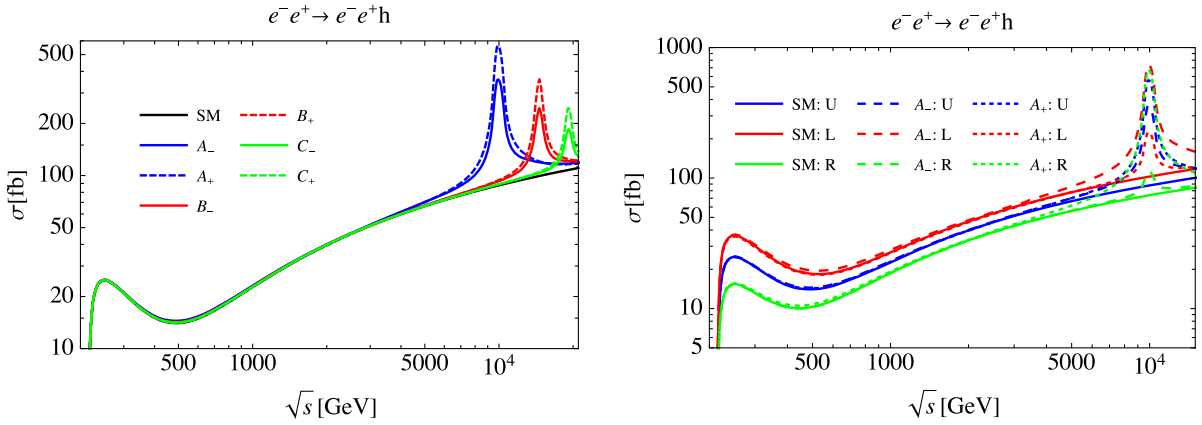

FIG. 8. The $\sqrt{s}$ dependence of the total cross sections of the $e^-e^+ \to e^-e^+h$ process with unpolarized and polarized electron and positron beams in the SM and the GHU model are shown. Other information is the same as in Fig. 4.

positron beams in the SM and the GHU model whose parameter sets are $A_\pm$. In both the figures, the main contribution to the peak around $\sqrt{s} \simeq 250$ GeV comes from the $e^-e^+ \to Z \to Zh \to e^-e^+h$ process, and the main contributions to the peaks around $O(10)$ TeV come from the $e^-e^+ \to Z'(= Z^{(1)}, Z_R^{(1)}) \to Zh \to e^-e^+h$ process for each parameter set. We verify that the contribution to the $e^-e^+ \to e^-e^+h$ process from the KK gauge bosons is small, independent of the KK masses and initial polarization of the electron and the positrons, except around the Z' boson mass scale.

From Figs. 4 and 8, we confirm that the cross section of the $e^-e^+ \to \nu\bar{\nu}h$ process is larger than that of the $e^-e^+ \to e^-e^+h$ process, unless the initial polarization is extremely right-handed polarization since the coupling constants of the W boson to the left-handed leptons are larger than the coupling constants of the Z boson to leptons.

In Fig. 9, the $\sqrt{s}$ dependence of the total cross sections of the $e^-e^+ \to e^-e^+h$ process in the SM and the GHU model whose parameter set is A_- with unpolarized electron and positron beams are shown up to $\sqrt{s} = 1$ TeV. There is almost no difference between the cross sections in the SM and the GHU model. In both the SM and the GHU model, the main contribution comes from the Zh process below $\sqrt{s} \simeq 500$ GeV, while the main contribution comes from the VBF process above $\sqrt{s} \simeq 500$ GeV, where the contributions from the Zh and VBF processes depend on the initial polarizations of the electron and the positron.

In Fig. 10, the $\sqrt{s}$ dependence of the deviation from the SM in the GHU model with six parameter sets $A_\pm$, $B_\pm$, $C_\pm$ for the total cross sections $\Delta_\sigma^{eeh}(P_{e^-}, P_{e^+})$ are shown. As the same as in Fig. 6, the left and right figures show the center-of-mass energies $\sqrt{s} = [200, 1000]$ GeV and $(P_{e^-}, P_{e^+}) = (-0.8, +0.3)$ and $(+0.8, -0.3)$, respectively. The 1σ statistical errors are estimated in the SM at each $\sqrt{s}$ with 1 ab^{-1} by using the decay mode of the Higgs boson h to two photons $\gamma\gamma$, where the branching ratio for the SM Higgs boson with $m_H = 125$ GeV is given by $\mathrm{Br}(h \to \gamma\gamma) = 2.27(1 \pm 0.021) \times 10^{-3}$ [16].

In Fig. 11, the $\sqrt{s}$ dependence of the left-right asymmetry $A_{LR}^{eeh}(P_{e^-}, P_{e^+})$ and the deviation from the SM of the left-right asymmetry $\Delta_{A_{LR}}^{eeh}(P_{e^-}, P_{e^+})$ with

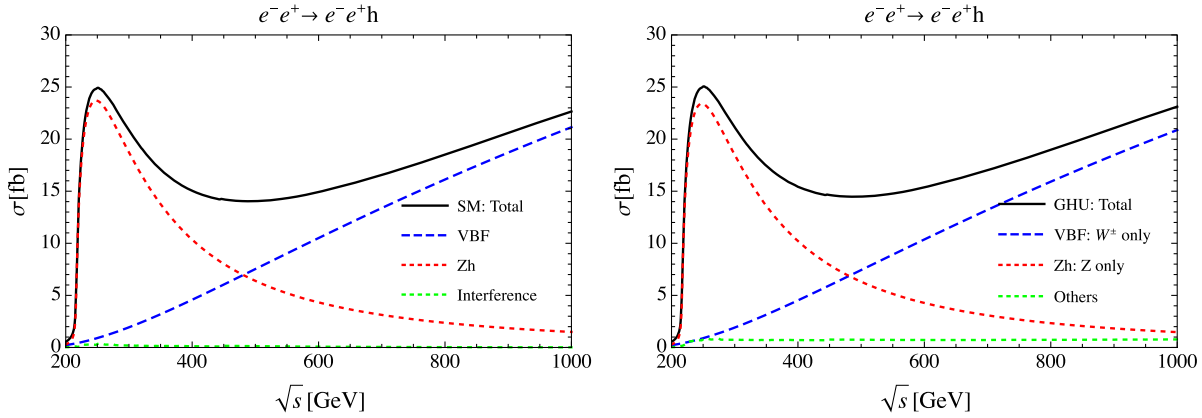

FIG. 9. The $\sqrt{s}$ dependence of the total cross sections of the $e^-e^+ \to e^-e^+h$ process with unpolarized electron and positron beams in the SM and the GHU model are shown for the left and right figures, respectively. Other information is the same as in Fig. 5.

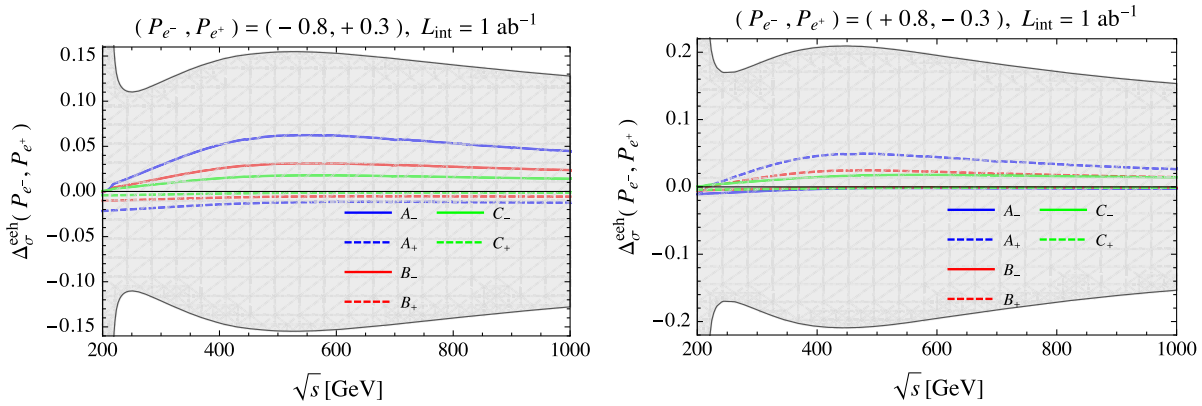

FIG. 10. The deviations from the SM in the GHU model with six parameter sets $A_\pm$, $B_\pm$, $C_\pm$ for total cross sections $\Delta^{eeh}_{\sigma}(P_{e^-}, P_{e^+})$ are shown for $\sqrt{s} = [200, 1000]$ GeV and $(P_{e^-}, P_{e^+}) = (-0.8, +0.3)$ and $(+0.8, -0.3)$, respectively. Other information is the same as in Fig. 6.

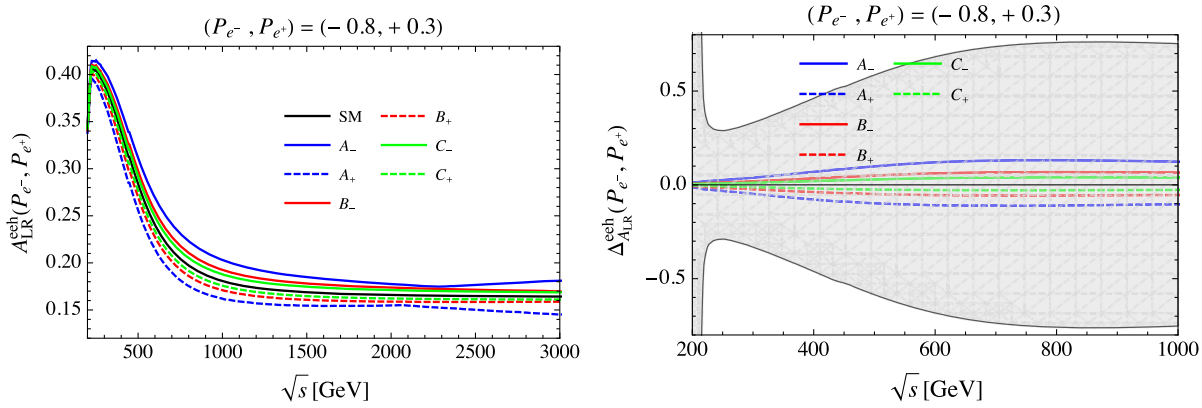

FIG. 11. The left-right asymmetry of the $e^-e^- \to e^-e^+h$ process and the deviation of the left-right asymmetry $\Delta^{eeh}_{A_{LR}}(P_{e^-}, P_{e^+})$ from the SM are shown. Other information is the same as in Fig. 7.

$(P_{e^-}, P_{e^+}) = (-0.8, +0.3)$ are shown, where $A^{eeh}_{LR}(P_{e^-}, P_{e^+})$ and $\Delta^{eeh}_{A_{LR}}(P_{e^-}, P_{e^+})$ are given in Eqs. (A46) and (A48). Although the deviation from the SM of the left-right asymmetry is quite large, but the number of events are small due to the small cross section. Therefore, it it very difficult to confirm the deviation from the SM by using the left-right asymmetry of the $e^-e^+ \to e^-e^+h$ process.

V. SUMMARY AND DISCUSSIONS

In this paper, we analyzed the three main single Higgs boson production processes $e^-e^+ \to Zh$, $e^-e^+ \to \nu\bar{\nu}h$, and $e^-e^+ \to e^-e^+h$. For the Higgs strahlung process $e^-e^+ \to Zh$, we showed that for a parameter region satisfying the current experimental constraints ($m_{\rm KK} \geq 13$ TeV, $\theta_H \leq 0.10$), a maximum deviation from the SM is about up to 6% for $\sqrt{s} = 250$ GeV and that from the SM is about up to 20% for $\sqrt{s} = 500$ GeV, depending on the initial polarizations of the electron and the positron. The deviation from the SM in the GHU model is monotonically increasing with respect to $\sqrt{s} \lesssim 1$ TeV. By observing the decay mode of the Z boson to the muon pair for $\sqrt{s} = 250$ GeV, $L_{\rm int} = 1$ ab^{-1}, and $(P_{e^-}, P_{e^+}) = (\mp 0.8, \pm 0.3)$, the deviation from the SM is larger than 3σ for $m_{\rm KK} \gtrsim 15$ TeV. By observing the decay mode of the Z boson to the muon pair for $\sqrt{s} = 500$ GeV, $L_{\rm int} = 2$ ab^{-1}, and $(P_{e^-}, P_{e^+}) = (\mp 0.8, \pm 0.3)$, the deviation from the SM is larger than 3σ for $m_{\rm KK} \gtrsim 20$ TeV. We also showed that the sign of the bulk mass of the electron multiplet in the GHU model can be determined by examining the deviation of the left-right symmetry of the $e^-e^+ \to Zh$ process from the SM. The $e^-e^+ \to \nu\bar{\nu}h$ process gives the main contribution to the single Higgs boson production at sufficiently high $\sqrt{s}$, but in the GHU model a sufficiently large deviation from the SM can only be observed at energy scales close to the Z' boson mass.

Although we focuses on single Higgs boson production processes in this paper, double Higgs boson production processes are important to determine the self-coupling constant of the Higgs boson because we need to confirm

whether the currently observed Higgs boson fully satisfies the properties of the Higgs boson predicted by the SM or not. In the GHU model, it is shown in Ref. [32] that the coupling constants of the Higgs boson to the W and Z bosons are very close to those in the SM, while the cubic and quartic self-coupling constants of the Higgs boson in the GHU model are deviated from those in the SM for about 8% and 30%, respectively. According to Ref. [110], the total cross section of the main double Higgs boson production $e^-e^+ \to Zhh$ at $\sqrt{s} = 500$ GeV is about 0.1 fb, where the main contribution comes from the $e^-e^+ \to Zh \to Zhh$ process. Even if almost all the decay modes of the Higgs boson could be used in the analysis, the 1σ statistical error of the $e^-e^+ \to Zhh$ process is about 5% by the ILC experiment with $\sqrt{s} = 500$ GeV and $L_{\rm int} = 4$ ab^{-1}. Therefore, it is difficult to check the deviation from the SM in the GHU model at the ILC experiment. The planned experiments at higher $\sqrt{s}$, such as the CLIC experiment, may confirm the deviation of the self-coupling constant of the Higgs boson from the SM by using a double Higgs boson production process $e^-e^+ \to \nu_e\bar{\nu}_e hh$ because the cross section of the process becomes larger when $\sqrt{s}$ becomes larger, where the main contribution comes from the $e^-e^+ \to \nu_e\bar{\nu}_e W^+W^- \to \nu_e\bar{\nu}_e h \to \nu_e\bar{\nu}_e hh$ process.

We comment on electroweak precision measurements. In this paper, we focus on the search for the GHU model by using the single Higgs boson production processes. By comparing the exploration region of the KK mass in the GHU model by using the single Higgs boson production processes with that by using the fermion pair production processes analyzed in Ref. [33], we find that fermion pair production processes can be explored to higher KK mass scale. Therefore, the first sign of the new physics in the ILC experiment is expected to be found not in the Higgs boson production process but in the fermion pair production processes because the cross section in the electron-positron collider experiments is larger for the fermion pair production processes than for the single Higgs boson production processes. This analysis of the Higgs boson production process provides one important piece of information to distinguish the GHU model from other new physics models.

ACKNOWLEDGMENTS

The authors would like to thank Yutaka Hosotani for useful discussions and comments. One of the authors (N. Y.) would like to thank Cheng-Wei Chiang for valuable comments. This work was supported in part by European Regional Development Fund-Project Engineering Applications of Microworld Physics (No. CZ.02.1.01/0.0/0.0/16_019/0000766) (Y. O.), and the Ministry of Science and Technology of Taiwan under Grant No. MOST-111-2811-M-002-047-MY2 (N. Y.).

APPENDIX: CROSS SECTION

In this section, we give the formulas necessary to calculate observables of the $e^-e^+ \to Zh$ and $e^-e^+ \to f\bar{f}h$ processes, where $f\bar{f}$ stands for a pair of fermions such as the electron and the positron (e^-e^+).

1. Cross section of $e^-e^+ \to Zh$

In the SM, the contribution to the cross section of $e^-e^+ \to Zh$ comes from the $e^-e^+ \to Z \to Zh$ process at tree level. In the GHU model, additional contributions come from not only the $e^-e^+ \to Z' \to Zh$ process but also the interference between the $e^-e^+ \to Z \to Zh$ process and the $e^-e^+ \to Z' \to Zh$ process.

a. Amplitude of $e^-e^+ \to Zh$

The s-channel production process of Zh via vector bosons $V_a = Z, Z'$ is given by

$$\begin{aligned} e^-_X(p_{e^-})e^+_{\bar{X}}(p_{e^+}) &\to V_a(q = p_{e^-} + p_{e^+} = p_Z + p_h) \\ &\to Z(p_Z)h(p_h), \end{aligned} \tag{A1}$$

where $X = L,\ R,\ \bar{L} = R,\ \bar{R} = L$. The amplitude of the $e^-e^+ \to Zh$ process is given by

$$\mathcal{M}^X = J^X_\mu \epsilon^{\mu *}(p_Z) Q_X, \tag{A2}$$

where ϵ^μ is a polarization vector of the finial state of the Z boson, J^X_μ is the fermion current defined as

$$J^X_\mu \coloneqq \bar{v}(p_{e^+})\gamma_\mu P_X u(p_{e^-}), \tag{A3}$$

and

$$Q_X \coloneqq \sum_a \frac{g^X_{V_a e} g_{V_a Zh}}{(q^2 - m^2_{V_a}) + i m_{V_a}\Gamma_{V_a}}, \tag{A4}$$

where $X = L, R$; $P_{R/L} = (1 \pm \gamma_5)/2$; $g^L_{V_a e}$ and $g^R_{V_a e}$ are the coupling constants of the left- and right-handed electron (the right- and left-handed positron) to the gauge boson V_a, respectively; $g_{V_a Zh}$ is the coupling constant of the gauge bosons V_a and Z to the Higgs boson h; m_{V_a} and Γ_{V_a} are the mass and the total decay width of V_a.

b. Kinematics of $e^-e^+ \to Zh$

We use the following four moments for the initial state of the electron (e^-) and the positron (e^+), and the final state of the Z boson (Z) and the Higgs boson (h) in the center-of-mass system:

$$
\begin{aligned}
p_{e^-} &= \frac{\sqrt{s}}{2}(1,0,0,+1), \qquad p_{e^+} = \frac{\sqrt{s}}{2}(1,0,0,-1) \\
p_Z &= (E_Z, +\kappa\sin\theta, 0, +\kappa\cos\theta), \qquad p_h = (E_h, -\kappa\sin\theta, 0, -\kappa\cos\theta), \\
q &= (\sqrt{s}, 0, 0, 0),
\end{aligned} \tag{A5}
$$

where we neglect the mass of electron; m_Z and m_h stand for the masses of the Z boson and the Higgs boson, respectively;

$$
\begin{aligned}
\kappa &:= \frac{\sqrt{[s-(m_Z+m_h)^2][s-(m_Z-m_h)^2]}}{2\sqrt{s}} = \frac{\lambda^{1/2}(s, m_Z^2, m_h^2)}{2\sqrt{s}}, \\
\lambda(\alpha,\beta,\gamma) &:= \alpha^2+\beta^2+\gamma^2-2\alpha\beta-2\alpha\gamma-2\beta\gamma = (\alpha-\beta-\gamma)^2-4\beta\gamma.
\end{aligned} \tag{A6}
$$

From the above, we find

$$
(p_{e^-}\cdot p_Z) = \frac{s}{2}(E_Z - p\cos\theta), \qquad (p_{e^+}\cdot p_Z) = \frac{s}{2}(E_Z + p\cos\theta). \tag{A7}
$$

The Mandelstam variables are given by

$$
\begin{aligned}
s &= (p_{e^-}+p_{e^+})^2 = (p_Z+p_h)^2 = q^2, \qquad t = (p_{e^-}-p_Z)^2 = (p_{e^+}-p_h)^2 = m_Z^2 - \sqrt{s}(E_Z - \kappa\cos\theta), \\
u &= (p_{e^-}-p_h)^2 = (p_{e^+}-p_Z)^2 = m_Z^2 - \sqrt{s}(E_Z + \kappa\cos\theta), \qquad s+t+u = m_Z^2+m_h^2.
\end{aligned} \tag{A8}
$$

c. Cross section of $e^-e^+ \to Zh$

For the $e_X^- e_{\bar{X}}^+ \to Zh$ process, when only vector bosons are involved in the intermediate states, the cross section of the initial states of the polarized electron and positron is given by

$$
\frac{d\sigma^{Zh}}{d\cos\theta}(P_{e^-}, P_{e^+}, \cos\theta) = \frac{1}{4}\left\{(1-P_{e^-})(1+P_{e^+})\frac{d\sigma_L^{Zh}}{d\cos\theta}(\cos\theta) + (1+P_{e^-})(1-P_{e^+})\frac{d\sigma_R^{Zh}}{d\cos\theta}(\cos\theta)\right\}, \tag{A9}
$$

where P_{e^-} and P_{e^+} are the initial polarizations of the electron and the positron, and σ_L^{Zh} and σ_R^{Zh} are cross sections of $e_L^- e_R^+ \to Zh$ and $e_R^- e_L^+ \to Zh$, respectively:

$$
\frac{d\sigma_X^{Zh}}{d\cos\theta}(\cos\theta) := \frac{d\sigma}{d\cos\theta}(e_X^- e_{\bar{X}}^+ \to Zh) = \frac{\kappa}{16\pi s\sqrt{s}}|\mathcal{M}^X|^2, \tag{A10}
$$

where the formula for the differential cross section in the SM is given in, e.g., Refs. [16,111]. The amplitude of the $e_X^- e_{\bar{X}}^+ \to Zh$ process can be obtained by using the standard method of calculation given in e.g., Ref. [111] as

$$
|\mathcal{M}^X|^2 = |Q_X|^2 s\frac{2m_Z^2+\kappa^2\sin^2\theta}{m_Z^2}, \tag{A11}
$$

where $Q_{X=L,R}$ are defined in Eq. (A4). Therefore, we find the differential cross section of the $e^-(P_{e^-})e^+(P_{e^+}) \to Zh$ process with the initial polarizations $P_{e^\pm}$ as

$$
\frac{d\sigma^{Zh}}{d\cos\theta}(P_{e^-}, P_{e^+}, \cos\theta) = \frac{1}{4}\left((1-P_{e^-})(1+P_{e^+})|Q_L|^2 + (1+P_{e^-})(1-P_{e^+})|Q_R|^2\right)\frac{\kappa}{16\pi\sqrt{s}}\frac{2m_Z^2+\kappa^2\sin^2\theta}{m_Z^2}. \tag{A12}
$$

The total cross section of the $e^-e^+ \to Zh$ process with the initial polarizations can be defined by integrating the differential cross section in Eq. (A9) with the angle θ

$$
\sigma^{Zh}(P_{e^-}, P_{e^+}) := \int_{-1}^{1}\frac{d\sigma^{Zh}}{d\cos\theta}(P_{e^-}, P_{e^+}, \cos\theta)d\cos\theta, \tag{A13}
$$

where the minimum and maximal values of $\cos\theta$ are determined by each detector and we cannot use date near $\cos\theta \simeq \pm 1$. By using Eq. (A12), the total cross section of $e^-e^+ \to Zh$ is given by

$$\sigma^{Zh}(P_{e^-}, P_{e^+}) = \frac{1}{4}(1-P_{e^-})(1+P_{e^+})\sigma_L^{Zh} + \frac{1}{4}(1+P_{e^-})(1-P_{e^+})\sigma_R^{Zh}, \quad \text{(A14)}$$

where

$$\sigma_X^{Zh} := \int_{-1}^{1} \frac{d\sigma_X^{Zh}}{d\cos\theta}(\cos\theta) d\cos\theta = |Q_X|^2 \frac{\kappa}{12\pi\sqrt{s}} \frac{3m_Z^2+\kappa^2}{m_Z^2}, \quad \text{(A15)}$$

where $X = L, R$; Q_X is given in Eq. (A4).

The statistical error of the cross section $\sigma^{Zh}(P_{e^-}, P_{e^+})$ is given by

$$\Delta\sigma^{Zh}(P_{e^-}, P_{e^+}) = \frac{\sigma^{Zh}(P_{e^-}, P_{e^+})}{\sqrt{N^{Zh}}}, \quad N^{Zh} = L_{\rm int} \cdot \sigma^{Zh}(P_{e^-}, P_{e^+}), \quad \text{(A16)}$$

where $L_{\rm int}$ is an integrated luminosity, and N^{Zh} is the number of events for the $e^-e^+ \to Zh$ process. Note that the Z boson and the Higgs boson cannot observed directly, so we need to choose the decay modes of the Z boson and/or the Higgs boson, and then the available number of events must be N^{Zh} multiplied by the branching ratio of each selected decay mode. The amount of the deviation of the cross section of the $e^-e^+ \to Zh$ process from the SM in the GHU model is given by

$$\Delta_\sigma^{Zh}(P_{e^-}, P_{e^+}) := \frac{[\sigma^{Zh}(P_{e^-}, P_{e^+})]_{\rm GHU}}{[\sigma^{Zh}(P_{e^-}, P_{e^+})]_{\rm SM}} - 1, \quad \text{(A17)}$$

where $[\sigma^{Zh}(P_{e^-}, P_{e^+})]_{\rm GHU}$ and $[\sigma^{Zh}(P_{e^-}, P_{e^+})]_{\rm SM}$ stand for the cross sections of the $e^-e^+ \to Zh$ process in the SM and the GHU model, respectively. The same notation is used for other cases in the followings.

d. Left-right asymmetry of $e^-e^+ \to Zh$

As the same in fermion pair productions, we can define a left-right asymmetry [33,36,86,87,93] of the $e^-e^+ \to Zh$ process as

$$A_{LR}^{Zh} := \frac{\sigma_L^{Zh} - \sigma_R^{Zh}}{\sigma_L^{Zh} + \sigma_R^{Zh}} = \frac{|Q_L|^2 - |Q_R|^2}{|Q_L|^2 + |Q_R|^2}, \quad \text{(A18)}$$

where σ_X^{Zh} and Q_X ($X = L, R$) are given in Eqs. (A4) and (A15), respectively.

An observable left-right asymmetry is defined as

$$A_{LR}^{Zh}(P_{e^-}, P_{e^+}) := \frac{\sigma^{Zh}(P_{e^-}, P_{e^+}) - \sigma^{Zh}(-P_{e^-}, -P_{e^+})}{\sigma^{Zh}(P_{e^-}, P_{e^+}) + \sigma^{Zh}(-P_{e^-}, -P_{e^+})} \quad \text{(A19)}$$

for $P_{e^-} < 0$ and $|P_{e^-}| > |P_{e^+}|$. From Eq. (A12), we find

$$A_{LR}^{Zh}(P_{e^-}, P_{e^+}, \cos\theta) = -\frac{P_{e^-} - P_{e^+}}{1 - P_{e^-}P_{e^+}} \frac{|Q_L|^2 - |Q_R|^2}{|Q_L|^2 + |Q_R|^2}. \quad \text{(A20)}$$

The relation between the theoretically defined left-right asymmetry A_{LR}^{Zh} given in Eq. (A18) and the observable left-right asymmetry $A_{LR}^{Zh}(P_{e^-}, P_{e^+})$ given in Eq. (A20) is given by

$$A_{LR}^{Zh} = \frac{1}{-P_{\rm eff}} A_{LR}^{Zh}(P_{e^-}, P_{e^+}), \qquad P_{\rm eff} := \frac{P_{e^-} - P_{e^+}}{1 - P_{e^-}P_{e^+}}. \quad \text{(A21)}$$

The statistical error of the left-right asymmetry is given by

$$\Delta A_{LR}^{Zh} = 2\frac{\sqrt{N_L^{Zh}N_R^{Zh}}\left(\sqrt{N_L^{Zh}} + \sqrt{N_R^{Zh}}\right)}{(N_L^{Zh} + N_R^{Zh})^2}, \quad \text{(A22)}$$

where $N_L^{Zh} = L_{\rm int}\sigma^{Zh}(P_{e^-}, P_{e^+})$ and $N_R^{Zh} = L_{\rm int}\sigma^{Zh}(-P_{e^-}, -P_{e^+})$ are the numbers of the events for $P_{e^-} < 0$ and $|P_{e^-}| > |P_{e^+}|$. The amount of the deviation from the SM in Eq. (A18) is characterized by

$$\Delta_{A_{LR}}^{Zh} := \frac{[A_{LR}^{Zh}]_{\rm GHU}}{[A_{LR}^{Zh}]_{\rm SM}} - 1. \quad \text{(A23)}$$

2. Cross section of $e^-e^+ \to f\bar{f}h$

The cross sections of the $e^-e^+ \to \nu\bar{\nu}h$ process via the $W^\pm$ bosons and of the $e^-e^+ \to e^-e^+h$ process via the Z bosons are estimated in Refs. [112–114]. When we consider the cross section of the $e^-e^+ \to f\bar{f}h$ processes ($f\bar{f} = \nu\bar{\nu}, e^-e^+$) in the SM, we need to take into account not only the vector boson fusion process $e^-e^+ \to f\bar{f}VV \to f\bar{f}h$ but also the Zh process $e^-e^+ \to Z \to Zh \to f\bar{f}h$. In the GHU model, additional contributions come from the W' and Z' bosons.

a. Amplitude of $e^-e^+ \to f\bar{f}VV \to f\bar{f}h$

The Higgs boson production processes via vector gauge bosons $V_a = W^{(\prime)\pm}$ or $Z^{(\prime)}$ are given by

$$e^-_X(p_1)e^+_Y(p_2) \to \nu_e(p_3)\bar{\nu}_e(p_4)W^{(\prime)-}(q_1 = p_1 - p_3)W^{(\prime)+}(q_2 = p_2 - p_4) \to \nu_e(p_3)\bar{\nu}_e(p_4)h(p_h)$$
$$e^-_X(p_1)e^+_Y(p_2) \to e^-(p_3)e^+(p_4)Z^{(\prime)}(q_1 = p_1 - p_3)Z^{(\prime)}(q_2 = p_2 - p_4) \to e^-(p_3)e^+(p_4)h(p_h), \tag{A24}$$

where $X, Y = L, R$; $\bar{L} = R, \bar{R} = L$; p_1 and p_2 are the momenta of the initial states of electron and positron; p_3 and p_4 are the momenta of the final states of fermions; and p_h is the momenta of the Higgs boson. The amplitude is given by

$$\mathcal{M}^{XY}_{VVh} = \sum_{V_a,V_b=\{W^{(\prime)}\}\text{ or }\{Z^{(\prime)}\}} g_{V_aV_bh} g^X_{V_ae} g^Y_{V_be} g^{\mu\nu} J^{XY}_{\mu\nu} \frac{1}{(q_1^2 - m^2_{V_a}) + i m_{V_a}\Gamma_{V_a}} \frac{1}{(q_2^2 - m^2_{V_b}) + i m_{V_b}\Gamma_{V_b}}, \tag{A25}$$

where we defined

$$J^{XY}_{\mu\nu} \coloneqq \bar{u}(p_3)\gamma_\mu P_X u(p_1)\bar{v}(p_2)\gamma_\nu P_Y v(p_4), \tag{A26}$$

and $P_{R/L} = (1 \pm \gamma_5)/2$. We neglected electron and neutrino masses.

After some tedious calculations, we obtain

$$\sum_{\text{spin}} |\mathcal{M}^{XY}_{VVh}|^2 = 16 \sum_{V_a,V_b,V_c,V_d=\{W^{(\prime)}\}\text{ or }\{Z^{(\prime)}\}} g_{V_aV_bh} g^*_{V_cV_dh} \times \left\{ \begin{array}{ll} g^X_{V_ae} g^X_{V_be} g^{X*}_{V_ce} g^{X*}_{V_de} (p_1 \cdot p_2)(p_3 \cdot p_4) & \text{for } X = Y \\ g^X_{V_ae} g^Y_{V_be} g^{X*}_{V_ce} g^{Y*}_{V_de} (p_1 \cdot p_4)(p_2 \cdot p_3) & \text{for } X \neq Y \end{array} \right\}$$
$$\times \frac{1}{(q_1^2 - m^2_{V_a}) + i m_{V_a}\Gamma_{V_a}} \frac{1}{(q_2^2 - m^2_{V_b}) + i m_{V_b}\Gamma_{V_b}} \frac{1}{(q_1^2 - m^2_{V_c}) - i m_{V_c}\Gamma_{V_c}} \frac{1}{(q_2^2 - m^2_{V_d}) - i m_{V_d}\Gamma_{V_d}}. \tag{A27}$$

b. Amplitude of $e^-e^+ \to Z^{(\prime)} \to Z^{(\prime)}h \to f\bar{f}h$

The Higgs boson production processes via neutral gauge bosons $V_a = Z, Z'$ are given by

$$e^-_X(p_1)e^+_Y(p_2) \to Z^{(\prime)}(q'_1 = p_1 + p_2) \to Z^{(\prime)}(q'_2 = p_3 + p_4)h(p_h) \to \nu(p_3)\bar{\nu}(p_4)h(p_h),$$
$$e^-_X(p_1)e^+_Y(p_2) \to Z^{(\prime)}(q'_1 = p_1 + p_2) \to Z^{(\prime)}(q'_2 = p_3 + p_4)h(p_h) \to e^-(p_3)e^+(p_4)h(p_h), \tag{A28}$$

The amplitude is given by

$$\mathcal{M}^{XY}_{Zh} = \sum_{V_a,V_b=\{Z^{(\prime)}\}} g_{V_aV_bh} g^X_{V_ae} g^Y_{V_be} g^{\mu\nu} J'^{XY}_{\mu\nu} \frac{1}{(q_1'^2 - m^2_{V_a}) + i m_{V_a}\Gamma_{V_a}} \frac{1}{(q_2'^2 - m^2_{V_b}) + i m_{V_b}\Gamma_{V_b}}, \tag{A29}$$

where we define $J'^{XY}_{\mu\nu}$ $(X, Y = L, R)$ as

$$J'^{XY}_{\mu\nu} = \bar{v}(p_2)\gamma_\mu P_X u(p_1)\bar{u}(p_3)\gamma_\nu P_Y v(p_4). \tag{A30}$$

By the same calculation as for the square of the amplitude given in Eq. (A27), we find

$$\sum_{\text{spin}} |\mathcal{M}^{XY}_{Zh}|^2 = 16 \sum_{V_a,V_b,V_c,V_d=\{Z^{(\prime)}\}} g_{V_aV_bh} g^*_{V_cV_dh} \times \left\{ \begin{array}{ll} g^X_{V_ae} g^X_{V_be} g^{X*}_{V_ce} g^{X*}_{V_de} (p_1 \cdot p_3)(p_2 \cdot p_4) & \text{for } X = Y \\ g^X_{V_ae} g^Y_{V_be} g^{X*}_{V_ce} g^{Y*}_{V_de} (p_1 \cdot p_4)(p_2 \cdot p_3) & \text{for } X \neq Y \end{array} \right\}$$
$$\times \frac{1}{(q_1'^2 - m^2_{V_a}) + i m_{V_a}\Gamma_{V_a}} \frac{1}{(q_2'^2 - m^2_{V_b}) + i m_{V_b}\Gamma_{V_b}} \frac{1}{(q_1'^2 - m^2_{V_c}) - i m_{V_c}\Gamma_{V_c}} \frac{1}{(q_2'^2 - m^2_{V_d}) - i m_{V_d}\Gamma_{V_d}}, \tag{A31}$$

where when the fermion pair in the final state is e^-e^+, $g^{L/R}_{V_be}$, and $g^{L/R}_{V_de}$ are gauge coupling constants of the left- or right-handed electron, while when the fermion pair in the final state is $\nu_e\bar{\nu}_e$, $g^{L/R}_{V_be}$ and $g^{L/R}_{V_de}$ are gauge coupling constants of the left-handed or right-handed neutrinos The $g^{L/R}_{V_ae}$ and $g^{L/R}_{V_ce}$ are always the gauge coupling constants of the left-handed or right-handed electron.

c. Interference of $e^-e^+ \to f\bar{f}VV \to f\bar{f}h$ and $e^-e^+ \to Z^{(\prime)} \to Z^{(\prime)}h \to f\bar{f}h$

The square of the amplitude of the $e_X^+ e_Y^- \to f\bar{f}h$ process is given by

$$|\mathcal{M}^{XY}|^2 = |\mathcal{M}^{XY}_{VVh} + \mathcal{M}^{XY}_{Zh}|^2 = |\mathcal{M}^{XY}_{VVh}|^2 + |\mathcal{M}^{XY}_{Zh}|^2 + 2\mathrm{Re}(\mathcal{M}^{XY}_{VVh}\mathcal{M}^{XY*}_{Zh}). \tag{A32}$$

The last term stands for the interference term between $e^-e^+ \to f\bar{f}VV \to f\bar{f}h$ and $e^-e^+ \to Z^{(\prime)} \to Z^{(\prime)}h \to f\bar{f}h$. This term also need to be calculated.

As the same as Eqs. (A25) and (A29), after some tedious calculations, we find

$$\begin{aligned}
2\mathrm{Re}\left[\sum_{\text{spin}} \mathcal{M}_{VVh}\mathcal{M}^*_{Zh}\right] = -16\mathrm{Re}\Bigg[& \sum_{V_a,V_b=\{W^{(\prime)}\}\text{ or }\{Z^{(\prime)}\}} \sum_{V_c,V_d=\{Z^{(\prime)}\}} g_{V_aV_bh} g^*_{V_c^*V_dh} \\
& \times \begin{Bmatrix} g^X_{V_ae} g^X_{V_be} g^{X*}_{V_ce} g^{X*}_{V_de} A + i g^X_{V_ae} g^X_{V_be} g^{X*}_{V_ce} g^{X*}_{V_de} B & \text{for } X = Y = L \\ g^X_{V_ae} g^X_{V_be} g^{X*}_{V_ce} g^{X*}_{V_de} A - i g^X_{V_ae} g^X_{V_be} g^{X*}_{V_ce} g^{X*}_{V_de} B & \text{for } X = Y = R \\ 0 & \text{for } X \neq Y \end{Bmatrix} \\
& \times \frac{1}{(q_1^2 - m^2_{V_a}) + i m_{V_a}\Gamma_{V_a}} \frac{1}{(q_2^2 - m^2_{V_b}) + i m_{V_b}\Gamma_{V_b}} \frac{1}{(q_1'^2 - m^2_{V_c}) - i m_{V_c}\Gamma_{V_c}} \frac{1}{(q_2'^2 - m^2_{V_d}) - i m_{V_d}\Gamma_{V_d}} \Bigg],
\end{aligned} \tag{A33}$$

where

$$A \coloneqq (p_1 \cdot p_4)(p_2 \cdot p_3) + (p_1 \cdot p_3)(p_2 \cdot p_4) - (p_1 \cdot p_2)(p_3 \cdot p_4), \qquad B \coloneqq p_1^\alpha p_2^\beta p_3^\gamma p_4^\delta \epsilon_{\gamma\beta\alpha\delta}. \tag{A34}$$

d. Kinematics of $e^-e^+ \to f\bar{f}h$

In the center-of-mass system of the initial electron and positron, the initial energies are $E_1 = E_2 = \sqrt{\hat{s}}/2$, where $\hat{s}$ is the center-of-mass energy for the initial electron and positron. When we take the same convention in Ref. [113], we define η and ζ as

$$E_3 = (1-\eta)\frac{1}{2}\sqrt{\hat{s}}, \qquad E_4 = (1-\zeta)\frac{1}{2}\sqrt{\hat{s}}, \tag{A35}$$

so that the energy of the Higgs boson is

$$E_h = (\eta + \zeta)\frac{1}{2}\sqrt{\hat{s}}. \tag{A36}$$

The final state momenta lie in a plane and

$$(\mathbf{p_h})^2 = (\mathbf{p}_3 + \mathbf{p}_4)^2 = E_h^2 - m_h^2. \tag{A37}$$

We define the angle of θ by

$$\cos\theta = -\hat{\mathbf{p}}_3 \cdot \hat{\mathbf{p}}_4 = 1 - 2\frac{\zeta\eta - \frac{m_h^2}{\hat{s}}}{(1-\zeta)(1-\eta)}. \tag{A38}$$

The kinematic boundaries occur for $\cos\theta = \pm 1$, and the allowed region must be satisfied as

$$\zeta\eta \geq \frac{m_h^2}{\hat{s}}, \qquad \zeta + \eta \leq 1 + \frac{m_h^2}{\hat{s}}. \tag{A39}$$

To specify the final state in the center-of-mass system of the initial electron and positron, we take the following basis:

$$\begin{aligned}
&\hat{\mathbf{p}}_1 = \hat{\mathbf{x}}, \qquad \hat{\mathbf{p}}_2 = -\hat{\mathbf{x}}, \qquad \hat{\mathbf{p}}_3 = \hat{\mathbf{x}}\cos\alpha\cos\beta + \hat{\mathbf{y}}\sin\alpha - \hat{\mathbf{z}}\sin\beta\cos\alpha, \\
&\hat{\mathbf{p}}_4 = -\hat{\mathbf{x}}\cos(\alpha-\theta)\cos\beta - \hat{\mathbf{y}}\sin(\alpha-\theta) + \hat{\mathbf{z}}\sin\beta\cos(\alpha-\theta).
\end{aligned} \tag{A40}$$

The Lorentz scalars are given as

$$
\begin{aligned}
(p_1 \cdot p_2) &= \frac{1}{2}\hat{s}, \qquad (p_2 \cdot p_3) = \frac{1}{4}(1-\eta)(1-\cos\alpha\sin\beta)\hat{s}, \\
(p_1 \cdot p_3) &= \frac{1}{4}(1-\eta)(1+\cos\alpha\sin\beta)\hat{s}, \qquad (p_3 \cdot p_4) = \frac{1}{4}(1-\zeta)(1-\eta)(1+\cos\theta)\hat{s}, \\
(p_1 \cdot p_4) &= \frac{1}{4}(1-\zeta)(1-\cos(\alpha-\theta)\sin\beta)\hat{s}, \qquad (p_2 \cdot p_4) = \frac{1}{4}(1-\zeta)(1+\cos(\alpha-\theta)\sin\beta)\hat{s}, \\
(q_1)^2 &= -\frac{1}{2}(1-\eta)(1+\cos\alpha\sin\beta)\hat{s}, \qquad (q_2)^2 = -\frac{1}{2}(1-\zeta)(1+\cos(\alpha-\theta)\sin\beta)\hat{s}, \\
(q_1')^2 &= \hat{s}, \qquad (q_2')^2 = \frac{1}{2}(1-\zeta)(1-\eta)(1+\cos\theta)\hat{s}.
\end{aligned} \tag{A41}
$$

e. Cross section of $e^-e^+ \to f\bar{f}h$

The differential cross section of the $e^-e^+ \to f\bar{f}h$ process is given by

$$
d\sigma^{ffh} = \frac{1}{16(2\pi)^4\hat{s}}|\mathcal{M}|^2 dE_3 dE_4 d\alpha d\cos\beta = \frac{1}{64(2\pi)^4}|\mathcal{M}|^2 d\eta d\zeta d\alpha d\cos\beta, \tag{A42}
$$

by using the formula in, e.g., Refs. [16,113]. The total cross section with the initial polarization of the electron and the positron is give by

$$
\begin{aligned}
\sigma^{ffh}(P_{e^-}, P_{e^+}) = \frac{1}{4}\{&(1-P_{e^-})(1+P_{e^+})\sigma_{LL}^{ffh} + (1+P_{e^-})(1-P_{e^+})\sigma_{RR}^{ffh} \\
&+ (1-P_{e^-})(1-P_{e^+})\sigma_{LR}^{ffh} + (1+P_{e^-})(1+P_{e^+})\sigma_{RL}^{ffh}\},
\end{aligned} \tag{A43}
$$

where

$$
\sigma_{XY}^{ffh} \coloneqq \frac{1}{64(2\pi)^4}\int_{\frac{m_h^2}{\hat{s}}}^{1} d\eta \int_{\frac{m_h^2}{\hat{s}\eta}}^{1+\frac{m_h^2}{\hat{s}}-\eta} d\zeta \int_0^{2\pi} d\alpha \int_{-1}^{1} d\cos\beta |\mathcal{M}^{XY}|^2, \tag{A44}
$$

where $|\mathcal{M}^{XY}|^2 (X, Y = L, R)$ are given by substituting Eqs. (A27), (A31), and (A33) into Eq. (A32). and we omitted $\sum_{\text{spin}}$ to simplify our notation.

The amount of the deviation of the cross section of the $e^-e^+ \to f\bar{f}h$ process from the SM in the GHU model is given by

$$
\Delta_\sigma^{ffh}(P_{e^-}, P_{e^+}) \coloneqq \frac{[\sigma^{ffh}(P_{e^-}, P_{e^+})]_{\text{GHU}}}{[\sigma^{ffh}(P_{e^-}, P_{e^+})]_{\text{SM}}} - 1, \tag{A45}
$$

where $[\sigma^{ffh}(P_{e^-}, P_{e^+})]_{\text{GHU}}$ and $[\sigma^{ffh}(P_{e^-}, P_{e^+})]_{\text{SM}}$ stand for the cross sections of the $e^-e^+ \to f\bar{f}h$ process in the SM and the GHU model, respectively.

f. Left-right asymmetry of $e^-e^+ \to f\bar{f}h$

Unlike the left-right asymmetry of the $e^-e^+ \to Zh$ process, we cannot define a left-right asymmetry of the $e^-e^+ \to f\bar{f}h$ process that does not depend on the initial polarization of electron and positron even if the off-shell particles are limited to vector bosons only. Still we can define a left-right asymmetry that depends on the initial polarization of the electron and the positron as

$$
A_{LR}^{ffh}(P_{e^-}, P_{e^+}) \coloneqq \frac{\sigma^{ffh}(P_{e^-}, P_{e^+}) - \sigma^{ffh}(-P_{e^-}, -P_{e^+})}{\sigma^{ffh}(P_{e^-}, P_{e^+}) + \sigma^{ffh}(-P_{e^-}, -P_{e^+})} \tag{A46}
$$

for $P_{e^-} < 0$ and $|P_{e^-}| > |P_{e^+}|$. By using Eq. (A43), we find

$$A_{LR}^{ffh}(P_{e^-},P_{e^+}) = -\frac{(P_{e^-}-P_{e^+})(\sigma_{LL}^{ffh}-\sigma_{RR}^{ffh})-(P_{e^-}+P_{e^+})(\sigma_{LR}^{ffh}-\sigma_{RL}^{ffh})}{(1-P_{e^-}P_{e^+})(\sigma_{LL}^{ffh}+\sigma_{RR}^{ffh})+(1+P_{e^-}P_{e^+})(\sigma_{LR}^{ffh}+\sigma_{RL}^{ffh})}. \tag{A47}$$

We can define the amount of the deviation from the SM in Eq. (A46) as

$$\Delta_{A_{LR}}^{ffh}(P_{e^-},P_{e^+}) \coloneqq \frac{[A_{LR}^{ffh}(P_{e^-},P_{e^+})]_{\mathrm{GHU}}}{[A_{LR}^{ffh}(P_{e^-},P_{e^+})]_{\mathrm{SM}}} - 1, \tag{A48}$$

where $[A_{LR}^{ffh}(P_{e^-},P_{e^+})]_{\mathrm{GHU}}$ and $[A_{LR}^{ffh}(P_{e^-},P_{e^+})]_{\mathrm{SM}}$ are $A_{LR}^{ffh}(P_{e^-},P_{e^+})$ in Eq. (A47) calculated with the parameter sets of the SM and the GHU model.

[1] G. Aad *et al.* (ATLAS Collaboration), The ATLAS experiment at the CERN large hadron collider, J. Instrum. **3**, S08003 (2008).

[2] S. Chatrchyan *et al.* (CMS Collaboration), The CMS experiment at the CERN LHC, J. Instrum. **3**, S08004 (2008).

[3] M. Cepeda *et al.*, Report from Working Group 2: Higgs physics at the HL-LHC and HE-LHC, CERN Yellow Rep. Monogr. **7**, 221 (2019).

[4] T. Behnke, J. E. Brau, B. Foster, J. Fuster, M. Harrison, J. M. Paterson, M. Peskin, M. Stanitzki, N. Walker, and H. Yamamoto, The international linear collider technical design report—volume 1: Executive summary, arXiv:1306.6327.

[5] H. Baer, T. Barklow, K. Fujii, Y. Gao, A. Hoang, S. Kanemura, J. List, H. E. Logan, A. Nomerotski, M. Perelstein *et al.*, The international linear collider technical design report—volume 2: Physics, arXiv:1306.6352.

[6] C. Adolphsen, M. Barone, B. Barish, K. Buesser, P. Burrows, J. Carwardine, J. Clark, H. Mainaud Durand, G. Dugan, E. Elsen *et al.*, The international linear collider technical design report—volume 3.I: Accelerator R&D in the technical design phase, arXiv:1306.6353.

[7] C. Adolphsen, M. Barone, B. Barish, K. Buesser, P. Burrows, J. Carwardine, J. Clark, H. Mainaud Durand, G. Dugan, E. Elsen *et al.*, The international linear collider technical design report—volume 3.II: Accelerator baseline design, arXiv:1306.6328.

[8] H. Abramowicz *et al.*, The international linear collider technical design report—volume 4: Detectors, arXiv:1306.6329.

[9] K. Fujii *et al.* (LCC Physics Working Group), Tests of the standard model at the international linear collider, arXiv:1908.11299.

[10] A. Aryshev *et al.* (ILC International Development Team), The international linear collider: Report to snowmass 2021, arXiv:2203.07622.

[11] L. Linssen, A. Miyamoto, M. Stanitzki, and H. Weerts, Physics and detectors at CLIC: CLIC conceptual design report, arXiv:1202.5940.

[12] A. Abada *et al.* (FCC Collaboration), FCC-hh: The hadron collider: Future circular collider conceptual design report volume 3, Eur. Phys. J. Spec. Top. **228**, 755 (2019).

[13] A. Blondel and P. Janot, FCC-ee overview: New opportunities create new challenges, Eur. Phys. J. Plus **137**, 92 (2022).

[14] S. Dasu *et al.*, Strategy for understanding the Higgs physics: The cool copper collider, arXiv:2203.07646.

[15] M. Dong *et al.* (CEPC Study Group), CEPC conceptual design report: Volume 2—physics & detector, arXiv:1811.10545.

[16] R. L. Workman *et al.* (Particle Data Group), Review of particle physics, Prog. Theor. Exp. Phys. **2022**, 083C01 (2022).

[17] Y. Hosotani, Dynamical mass generation by compact extra dimensions, Phys. Lett. B **126**, 309 (1983).

[18] Y. Hosotani, Dynamics of nonintegrable phases and gauge symmetry breaking, Ann. Phys. (N.Y.) **190**, 233 (1989).

[19] A. T. Davies and A. McLachlan, Gauge group breaking by Wilson loops, Phys. Lett. B **200**, 305 (1988).

[20] A. T. Davies and A. McLachlan, Congruency class effects in the Hosotani model, Nucl. Phys. **B317**, 237 (1989).

[21] H. Hatanaka, T. Inami, and C. S. Lim, The gauge hierarchy problem and higher dimensional gauge theories, Mod. Phys. Lett. A **13**, 2601 (1998).

[22] H. Hatanaka, Matter representations and gauge symmetry breaking via compactified space, Prog. Theor. Phys. **102**, 407 (1999).

[23] K. Agashe, R. Contino, and A. Pomarol, The minimal composite Higgs model, Nucl. Phys. **B719**, 165 (2005).

[24] A. D. Medina, N. R. Shah, and C. E. M. Wagner, Gauge-Higgs unification and radiative electroweak symmetry breaking in warped extra dimensions, Phys. Rev. D **76**, 095010 (2007).

[25] Y. Hosotani, K. Oda, T. Ohnuma, and Y. Sakamura, Dynamical electroweak symmetry breaking in $SO(5) \times U(1)$ gauge-Higgs unification with top and bottom quarks, Phys. Rev. D **78**, 096002 (2008).

[26] S. Funatsu, H. Hatanaka, Y. Hosotani, Y. Orikasa, and N. Yamatsu, GUT inspired $SO(5) \times U(1) \times SU(3)$ gauge-Higgs unification, Phys. Rev. D **99**, 095010 (2019).
[27] S. Funatsu, H. Hatanaka, Y. Hosotani, Y. Orikasa, and T. Shimotani, Novel universality and Higgs decay H $\to \gamma\gamma$, gg in the SO(5) $\times$ U(1) gauge-Higgs unification, Phys. Lett. B **722**, 94 (2013).
[28] S. Funatsu, H. Hatanaka, Y. Hosotani, Y. Orikasa, and T. Shimotani, LHC signals of the $SO(5) \times U(1)$ gauge-Higgs unification, Phys. Rev. D **89**, 095019 (2014).
[29] S. Funatsu, H. Hatanaka, and Y. Hosotani, $H \to Z\gamma$ in the gauge-Higgs unification, Phys. Rev. D **92**, 115003 (2015).
[30] S. Funatsu, H. Hatanaka, Y. Hosotani, and Y. Orikasa, Collider signals of W' and Z' bosons in the gauge-Higgs unification, Phys. Rev. D **95**, 035032 (2017).
[31] S. Funatsu, H. Hatanaka, Y. Hosotani, Y. Orikasa, and N. Yamatsu, CKM matrix and FCNC suppression in $SO(5) \times U(1) \times SU(3)$ gauge-Higgs unification, Phys. Rev. D **101**, 055016 (2020).
[32] S. Funatsu, H. Hatanaka, Y. Hosotani, Y. Orikasa, and N. Yamatsu, Effective potential and universality in GUT-inspired gauge-Higgs unification, Phys. Rev. D **102**, 015005 (2020).
[33] S. Funatsu, H. Hatanaka, Y. Hosotani, Y. Orikasa, and N. Yamatsu, Fermion pair production at e^-e^+ linear collider experiments in GUT Inspired gauge-Higgs unification, Phys. Rev. D **102**, 015029 (2020).
[34] S. Funatsu, H. Hatanaka, Y. Hosotani, Y. Orikasa, and N. Yamatsu, Electroweak and left-right phase transitions in $SO(5) \times U(1) \times SU(3)$ gauge-Higgs unification, Phys. Rev. D **104**, 115018 (2021).
[35] S. Funatsu, H. Hatanaka, Y. Hosotani, Y. Orikasa, and N. Yamatsu, Signals of W' and Z' bosons at the LHC in the $SU(3) \times SO(5) \times U(1)$ gauge-Higgs unification, Phys. Rev. D **105**, 055015 (2022).
[36] S. Funatsu, H. Hatanaka, Y. Hosotani, Y. Orikasa, and N. Yamatsu, Bhabha scattering in the gauge-Higgs unification, Phys. Rev. D **106**, 015015 (2022).
[37] E. Senaha, Symmetry restoration and breaking at finite temperature: An introductory review, Symmetry **12**, 733 (2020).
[38] Y. Hosotani and N. Yamatsu, Gauge-Higgs grand unification, Prog. Theor. Exp. Phys. **2015**, 111B01 (2015).
[39] N. Yamatsu, Gauge coupling unification in gauge-Higgs grand unification, Prog. Theor. Exp. Phys. **2016**, 043B02 (2016).
[40] A. Furui, Y. Hosotani, and N. Yamatsu, Toward realistic gauge-Higgs grand unification, Prog. Theor. Exp. Phys. **2016**, 093B01 (2016).
[41] Y. Hosotani and N. Yamatsu, Electroweak symmetry breaking and mass spectra in six-dimensional gauge-Higgs grand unification, Prog. Theor. Exp. Phys. **2018**, 023B05 (2018).
[42] Y. Hosotani and N. Yamatsu, Gauge-Higgs seesaw mechanism in 6-dimensional grand unification, Prog. Theor. Exp. Phys. **2017**, 091B01 (2017).
[43] C. Englert, D. J. Miller, and D. D. Smaranda, Phenomenology of GUT-inspired gauge-Higgs unification, Phys. Lett. B **802**, 135261 (2020).
[44] C. Englert, D. J. Miller, and D. D. Smaranda, The Weinberg angle and 5D RGE effects in a SO(11) GUT theory, Phys. Lett. B **807**, 135548 (2020).
[45] H. Georgi and S. L. Glashow, Unity of All Elementary Particle Forces, Phys. Rev. Lett. **32**, 438 (1974).
[46] K. Inoue, A. Kakuto, and Y. Nakano, Unification of the lepton-quark world by the gauge group SU(6), Prog. Theor. Phys. **58**, 630 (1977).
[47] H. Fritzsch and P. Minkowski, Unified interactions of leptons and hadrons, Ann. Phys. (N.Y.) **93**, 193 (1975).
[48] F. Gursey, P. Ramond, and P. Sikivie, A universal gauge theory model based on E_6, Phys. Lett. **60B**, 177 (1976).
[49] R. Slansky, Group theory for unified model building, Phys. Rep. **79**, 1 (1981).
[50] N. Yamatsu, Finite-dimensional Lie algebras and their representations for unified model building, arXiv:1511.08771.
[51] Y. Kawamura, Gauge symmetry breaking from extra space S^1/Z_2, Prog. Theor. Phys. **103**, 613 (2000).
[52] Y. Kawamura, Split multiplets, coupling unification and extra dimension, Prog. Theor. Phys. **105**, 691 (2001).
[53] Y. Kawamura, Triplet-doublet splitting, proton stability and extra dimension, Prog. Theor. Phys. **105**, 999 (2001).
[54] L. J. Hall and Y. Nomura, Gauge unification in higher dimensions, Phys. Rev. D **64**, 055003 (2001).
[55] L. J. Hall, Y. Nomura, and D. Tucker-Smith, Gauge Higgs unification in higher dimensions, Nucl. Phys. **B639**, 307 (2002).
[56] G. Burdman and Y. Nomura, Unification of Higgs and gauge fields in five-dimensions, Nucl. Phys. **B656**, 3 (2003).
[57] C. S. Lim and N. Maru, Towards a realistic grand gauge-Higgs unification, Phys. Lett. B **653**, 320 (2007).
[58] K. Kojima, K. Takenaga, and T. Yamashita, Grand gauge-Higgs unification, Phys. Rev. D **84**, 051701 (2011).
[59] K. Kojima, K. Takenaga, and T. Yamashita, Gauge symmetry breaking patterns in an SU(5) grand gauge-Higgs unification model, Phys. Rev. D **95**, 015021 (2017).
[60] K. Kojima, K. Takenaga, and T. Yamashita, The standard model gauge symmetry from higher-rank unified groups in grand gauge-Higgs unification models, J. High Energy Phys. 06 (2017) 018.
[61] N. Yamatsu, Special grand unification, Prog. Theor. Exp. Phys. **2017**, 061B01 (2017).
[62] N. Yamatsu, String-inspired special grand unification, Prog. Theor. Exp. Phys. **2017**, 101B01 (2017).
[63] N. Yamatsu, Family unification in special grand unification, Prog. Theor. Exp. Phys. **2018**, 091B01 (2018).
[64] N. Maru and Y. Yatagai, Fermion mass hierarchy in grand gauge-Higgs unification, Prog. Theor. Exp. Phys. **2019**, 083B03 (2019).
[65] Y. Kawamura, E. Kodaira, K. Kojima, and T. Yamashita, On representation matrices of boundary conditions in $SU(n)$ gauge theories compactified on two-dimensional orbifolds, arXiv:2211.00877.
[66] G. Aad *et al.* (ATLAS Collaboration), Search for high-mass dilepton resonances using 139 fb^{-1} of pp collision data collected at $\sqrt{s} = 13$ TeV with the ATLAS detector, Phys. Lett. B **796**, 68 (2019).

[67] G. Aad *et al.* (ATLAS Collaboration), Search for new non-resonant phenomena in high-mass dilepton final states with the ATLAS detector, J. High Energy Phys. 11 (2020) 005; 04 (2021) 142(E).
[68] G. Aad *et al.* (ATLAS Collaboration), Search for a heavy charged boson in events with a charged lepton and missing transverse momentum from pp collisions at $\sqrt{s} = 13$ TeV with the ATLAS detector, Phys. Rev. D **100**, 052013 (2019).
[69] G. Aad *et al.* (ATLAS Collaboration), Search for new resonances in mass distributions of jet pairs using 139 fb^{-1} of pp collisions at $\sqrt{s} = 13$ TeV with the ATLAS detector, J. High Energy Phys. 03 (2020) 145.
[70] A. M. Sirunyan *et al.* (CMS Collaboration), Search for high mass dijet resonances with a new background prediction method in proton-proton collisions at $\sqrt{s} = 13$ TeV, J. High Energy Phys. 05 (2020) 033.
[71] A. M. Sirunyan *et al.* (CMS Collaboration), Search for resonant and nonresonant new phenomena in high-mass dilepton final states at $\sqrt{s} = 13$ TeV, J. High Energy Phys. 07 (2021) 208.
[72] S. Funatsu, H. Hatanaka, Y. Hosotani, and Y. Orikasa, Distinct signals of the gauge-Higgs unification in e^+e^- collider experiments, Phys. Lett. B **775**, 297 (2017).
[73] J. Yoon and M. E. Peskin, Fermion pair production in $SO(5) \times U(1)$ gauge-Higgs unification models, arXiv:1811.07877.
[74] J. Yoon and M. E. Peskin, Dissection of an $SO(5) \times U(1)$ gauge-Higgs unification model, Phys. Rev. D **100**, 015001 (2019).
[75] S. Funatsu, Forward-backward asymmetry in the gauge-Higgs unification at the international linear collider, Eur. Phys. J. C **79**, 854 (2019).
[76] S. Bilokin, R. Pöschl, and F. Richard, Measurement of b quark EW couplings at ILC, arXiv:1709.04289.
[77] F. Richard, Bhabha scattering at ILC250, arXiv:1804.02846.
[78] A. Irles, R. Pöschl, F. Richard, and H. Yamamoto, Complementarity between ILC250 and ILC-GigaZ, in *Linear Collider Community Meeting Lausanne, Switzerland* 2019)), arXiv:1905.00220.
[79] A. Irles, R. Pöschl, and F. Richard, Production and measurement of $e^+e^- \to c\bar{c}$ signatures at the 250 GeV ILC, in *International Workshop on Future Linear Colliders (LCWS 2019), Japan* (2019), arXiv:2002.05805.
[80] K. Fujii *et al.*, Physics case for the 250 GeV stage of the international linear collider, arXiv:1710.07621.
[81] H. Aihara *et al.* (ILC Collaboration), The international linear collider. A global project, arXiv:1901.09829.
[82] P. Bambade *et al.*, The international linear collider: A global project, arXiv:1903.01629.
[83] R. Pöschl (ILC International Development Team Working Group 3), Top and heavy quark studies at linear colliders, Proc. Sci. EPS-HEP2021 (**2022**) 491.
[84] B. Schrempp, F. Schrempp, N. Wermes, and D. Zeppenfeld, Bounds on new contact interactions from future e^+e^- colliders, Nucl. Phys. **B296**, 1 (1988).
[85] D. C. Kennedy, B. W. Lynn, C. J. C. Im, and R. G. Stuart, Electroweak cross-sections and asymmetries at the Z^0, Nucl. Phys. **B321**, 83 (1989).
[86] K. Abe *et al.* (SLD Collaboration), Precise Measurement of the Left-Right Cross-Section Asymmetry in Z Boson Production by e^+e^- Collisions, Phys. Rev. Lett. **73**, 25 (1994).
[87] K. Abe *et al.* (SLD Collaboration), An Improved Measurement of the Left-Right Z^0 Cross-Section Asymmetry, Phys. Rev. Lett. **78**, 2075 (1997).
[88] A. Blondel, B. W. Lynn, F. M. Renard, and C. Verzegnassi, Precision measurements of final state weak coupling from polarized electron–positron annihilation, Nucl. Phys. **B304**, 438 (1988).
[89] K. Abe *et al.* (SLD Collaboration), Measurement of A_b and A_c from the Left-Right Forward-Backward Asymmetry of Leptons in Hadronic Events at the Z^0 Resonance, Phys. Rev. Lett. **74**, 2895 (1995).
[90] K. Abe *et al.* (SLD Collaboration), Measurement of A_b from the Left-Right Forward-Backward Asymmetry of b Quark Production in Z^0 Decays Using a Momentum-Weighted Track-Charge Technique, Phys. Rev. Lett. **74**, 2890 (1995).
[91] K. Abe *et al.* (SLD Collaboration), Measurement of the Left-Right Forward-Backward Asymmetry for Charm Quarks with D^{*+} and D^+ Mesons, Phys. Rev. Lett. **75**, 3609 (1995).
[92] K. Abe *et al.* (SLD Collaboration), Polarized Bhabha Scattering a Precision Measurement of the Electron Neutral Current Couplings, Phys. Rev. Lett. **74**, 2880 (1995).
[93] G. Moortgat-Pick *et al.*, The role of polarized positrons and electrons in revealing fundamental interactions at the linear collider, Phys. Rep. **460**, 131 (2008).
[94] S. Schael *et al.* (ALEPH, DELPHI, L3, OPAL, and LEP Electroweak Collaborations), Electroweak measurements in electron-positron collisions at W-boson-pair energies at LEP, Phys. Rep. **532**, 119 (2013).
[95] D. Bardin, Y. Dydyshka, L. Kalinovskaya, L. Rumyantsev, A. Arbuzov, R. Sadykov, and S. Bondarenko, One-loop electroweak radiative corrections to polarized bhabha scattering, Phys. Rev. D **98**, 013001 (2018).
[96] V. I. Borodulin, R. N. Rogalyov, and S. R. Slabospitskii, CORE 3.1 (COmpendium of RElations, Version 3.1), arXiv:1702.08246.
[97] A. Djouadi, The anatomy of electro-weak symmetry breaking. I: The Higgs boson in the standard model, Phys. Rep. **457**, 1 (2008).
[98] J. Yan, S. Watanuki, K. Fujii, A. Ishikawa, D. Jeans, J. Strube, J. Tian, and H. Yamamoto, Measurement of the Higgs boson mass and $e^+e^- \to ZH$ cross section using $Z \to \mu^+\mu^-$ and $Z \to e^+e^-$ at the ILC, Phys. Rev. D **94**, 113002 (2016).
[99] G. Belanger, F. Boudjema, J. Fujimoto, T. Ishikawa, T. Kaneko, K. Kato, and Y. Shimizu, Full one loop electroweak radiative corrections to single Higgs production in e^+e^-, Phys. Lett. B **559**, 252 (2003).
[100] F. Boudjema, J. Fujimoto, T. Ishikawa, T. Kaneko, K. Kato, Y. Kurihara, Y. Shimizu, and Y. Yasui, Electroweak corrections to Higgs production through ZZ fusion at the linear collider, Phys. Lett. B **600**, 65 (2004).
[101] A. Denner, S. Dittmaier, M. Roth, and M. M. Weber, Electroweak radiative corrections to single Higgs boson

production in e^+e^- annihilation, Phys. Lett. B **560**, 196 (2003).
[102] A. Denner, S. Dittmaier, M. Roth, and M. M. Weber, Electroweak radiative corrections to $e^+e^- \to \nu\bar{\nu}H$, Nucl. Phys. **B660**, 289 (2003).
[103] C.-x. Yue, S.-z. Wang, and D.-q. Yu, Littlest Higgs model and associated ZH production at high energy e^+e^- collider, Phys. Rev. D **68**, 115004 (2003).
[104] C.-X. Yue, W. Wang, Z.-J. Zong, and F. Zhang, Probing signals of the littlest Higgs model via the WW fusion processes at the high energy e^+e^- collider, Eur. Phys. J. C **42**, 331 (2005).
[105] X.-l. Wang, Y.-b. Liu, J.-h. Chen, and H. Yang, The correction of the littlest Higgs model to the Higgs production process $e^+e^- \to e^+e^-H$ at the ILC, Eur. Phys. J. C **49**, 593 (2007).
[106] J. Han, S. Li, B. Yang, and N. Liu, Higgs boson production and decay at e^+e^- colliders as a probe of the left-right twin Higgs model, Nucl. Phys. **B896**, 200 (2015).
[107] L. Randall and R. Sundrum, A Large Mass Hierarchy from a Small Extra Dimension, Phys. Rev. Lett. **83**, 3370 (1999).
[108] ALEPH, DELPHI, L3, OPAL, and SLD Collaborations, LEP Electroweak Working Group, and SLD Electroweak and Heavy Flavour Groups, Precision electroweak measurements on the Z resonance, Phys. Rep. **427**, 257 (2006).
[109] Z.-z. Xing, H. Zhang, and S. Zhou, Updated values of running quark and lepton masses, Phys. Rev. D **77**, 113016 (2008).
[110] H. Abramowicz *et al.*, Higgs physics at the CLIC electron–positron linear collider, Eur. Phys. J. C **77**, 475 (2017).
[111] M. E. Peskin and D. V. Schroeder, *An Introduction to Quantum Field Theory* (Addison-Wesley, Reading, USA, 1995), p. 842.
[112] D. R. T. Jones and S. T. Petcov, Heavy Higgs bosons at LEP, Phys. Lett. B **84**, 440 (1979).
[113] R. N. Cahn, Production of heavy Higgs Bosons: Comparisons of exact and approximate results, Nucl. Phys. **B255**, 341 (1985); **B262**, 744(E) (1985).
[114] G. Altarelli, B. Mele, and F. Pitolli, Heavy Higgs production at future colliders, Nucl. Phys. **B287**, 205 (1987).